STOCKHOLM UNIVERSITY
DEPARTMENT OF ASTRONOMY

MASTER OF SCIENCE THESIS

Planets Throughout Space & Time:

A cosmochronological look at terrestrial planets

Author:
Per Calissendorff
890303-0552
per.calissendorff@live.se

Supervisor:
Erik Zackrisson

May 21, 2015

"Those worlds in space are as countless as all the grains of sand on all the beaches of the earth. Each of those worlds is as real as ours and every one of them is a succession of incidents, events, occurrences which influence its future. Countless worlds, numberless moments, an immensity of space and time. And our small planet at this moment, here we face a critical branch point in history: what we do with our world, right now, will propagate down through the centuries and powerfully affect the destiny of our descendants. It is well within our power to destroy our civilization and perhaps our species as well."

-Carl Sagan, Cosmos: A Personal Voyage

Abstract

Exoplanetary astronomy is a flourishing field of study at the moment, with much thanks to the great success of missions such as *Kepler* and many more. Both observations and simulations entail to a correlation between the metallicity of the host star and the occurrence of very massive companions, i.e. giant planets. However, a comparable correlation is not found for smaller, rocky planets and the explanation for that remains ambiguous and debatable. Here, we assume the paucity for plentiful amount of terrestrial planets (defined here as planets with $R = 0.5-2.0R_{\oplus}$ or $M = 0.5-10M_{\oplus}$) at higher metallicities to be the cause of violent interactions with migrating giant planets. In our method we apply the most recent results of occurrence rates for exoplanets orbiting FGKM-stars in order to procure a *planet occurrence recipe*. We use semi-analytic models to predict the cosmic star formation history and chemical evolution of the observable Universe in order to make an assessment on the prevalence of terrestrial planets throughout cosmic times. In our analysis we find the most prosperous cosmic age for terrestrial planets to form around main sequence stars to be ≈ 7.8 Gyrs ago (i.e. at redshift $z \approx 1$). Through our calculations we estimate the number of terrestrial planets in the observable Universe to be $N_p \geqslant 6.61^{+12.79}_{-0.02} \times 10^{20}$. We believe these results to be further improved upon with the efforts of forthcoming exoplanet missions such as TESS, PLATO and more.

Acknowledgements

There are several people I would like to acknowledge for helping me bringing this project together. Thanks to Anders Johansen and Markus Jansson for their constructive feedback on my work. Thanks to Andrew Benson for providing the semi-analytic model and answering all questions related to it. And a great thank you goes to my supervisor Erik Zackrisson, for giving me the opportunity to work on such an appealing project.

Contents

Page

List of Figures

Page

List of Tables

While it may be disappointing, I have to confess to people who ask for my insights on the meaning of it all that astronomy doesn't provide any clearly useful data on matters of sin and souls.

-Seth Shostak

1

Introduction

ALTHOUGH being a fairly young discipline in astronomy, exoplanetary astronomy has been very fruitful since the first discovery of planets far away from our own Solar system some $\sim$ 20 odd years ago (Wolszczan & Frail 1992). Today, more than 1800 exoplanets have been confirmed [1] and many more exoplanet candidates are waiting for confirmation. The first discovery of an exoplanet orbiting a Sun-like star was made by Mayor & Queloz (1995) and serves as a celebrated milestone for exoplanetary astronomy. Perhaps one of the most confounding aspects of that discovery at the time was that the size of the planet was comparable to that of Jupiter but its orbital period was only a few days, meaning the planet was very close to its host stars. This seemingly exotic object was therefore named to be a *hot Jupiter* and very distinguishable from our previous knowledge about planetary systems. Indeed, the awareness that planetary systems may diverge substantially from our own became apparent. A question that arose from the discovery of hot Jupiters was, how did they get there? With our current understanding of planet formation there should not have been enough solid materials in the early protoplanetary disk to form hot Jupiters at their current place (e.g. Kley & Nelson 2012), or *in situ* as it is usually referred to. One explanation is that giant planets form far out and then migrate inwards, which could disclose their massive sizes. Thus, the theory of planet migration became increasingly more popular for explaining the occurrence of close in orbits for giant planets.

[1] http://exoplanetarchive.ipac.caltech.edu/ May 21, 2015

Due to the limitations on our observational techniques to find exoplanets we are often biased towards finding these hot Jupiters, making it reasonable that it would be one of the first kind of planet found outside our own Solar system. Actually, the shear size and short orbits make them perfect targets for our *Doppler* and transit observations. Nevertheless, as our techniques and knowledge improved we found that hot Jupiters are generally not accompanied by low-mass planets on nearby orbits (e.g. Steffen et al. 2012). Giant planets that migrate generally leave very little materials left for other planets to form in their wake (e.g. Armitage 2003). Studies by Fischer & Valenti (2005; hereafter FV05) Neves et al. (2013); Gaidos & Mann (2014; hereafter GM14) have shown that the occurrence of giant planets increases with the metallicity content of the host star. The strong dependence of giant planet frequency with stellar metallicity from FV05 is shown in Figure 1.1. Such correlation is not found for less-massive rocky planets which, according to Neves et al. (2013), are hinted to have an anti-correlation with stellar host metallicity instead. Lineweaver (2001; hereafter L01) attempted to estimate the prevalence of Earth-like planets around Solar-like stars through the argument that as the probability of having a hot Jupiter increases based on the metallicity of the host star, the probability to harbour an Earth-like planet decreases. If planet occurrence is determined by the metallicity of the host star, there may exist a *"sweet spot"* in host star metallicity where Earth-like planets have a better chance of surviving which we will investigate and discuss in this thesis.

Here, we adopt the same strategy devised by L01 in order to measure the number of terrestrial (planets with sizes roughly $0.5-2R_{\oplus}$ and $0.5-10M_{\oplus}$) planets in the observable Universe, i.e. in the past light cone of Earth now, as well as estimating the mean age of such planets. In our calculations we endorse more recent data of exoplanet occurrences made by missions and surveys such as *Kepler*, High Accuracy Radial-velocity Planet Searcher (HARPS) and the California Planet Survey (CPS). We use *semi-analytical models* of galaxy formation with the purpose of obtaining the star formation history of the Universe and its chemical evolution over a great range of redshifts. These parameters are quantised as a *planet occurrence recipe* which we apply in order to predict the number of terrestrial planets formed and anticipate how many would be destroyed and lost due to the migration of giant planets. If our assumptions hold true, we come to the conclusion that the Earth is relatively young for a terrestrial planet and that most planets are a few billion years older.

We also discuss the prescriptions for terrestrial planets to be habitable. Kasting et al. (1993) argued for a *habitable zone* (HZ) around host stars which could was required in order for terrestrial planets to be able to contain water in liquid form on its surface.

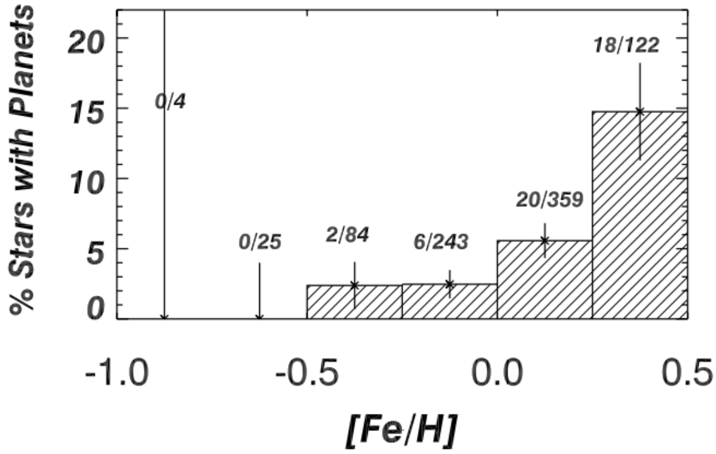

Figure 1.1: Metallicity correlation for the occurrence of giant planets from Doppler studies of massive companions with orbital periods < 4 years. The number above each bar on the histogram indicate the ratio of planets to stars in each bin. Courtesy of Fischer & Valenti (2005)

Nevertheless, that is but one requirement for a terrestrial planet to be habitable as we know it. There are many variations of theories regarding habitability (e.g. Kasting et al. 1993; Kopparapu et al. 2013), some which may also depend on how strict one sets the limits for habitability. It is not entirely certain that all of the criteria for habitability is applicable for all of the planets predicted by our model.

The approach of this thesis starts with some background regarding previous work on similar topics and some general theory about planet formation in Section 2. In the following Section 3, we go into more detail on the semi-analytical models and describe how we analyse the data and produce the results we get, which are given in Section 4. We explore the possibility for habitability in Section 4.5 and give our final conclusions with a discussion lastly in Section 5. Unless otherwise stated, the results presented here will have assumed a *"cosmic concordance cosmology"* with parameters $\Omega_M = 0.3$, $\Omega_\Lambda = 0.7$ and $h = 0.7$. We also infer a solar metallicity as $Z_\odot = 0.0152$.

Study the past, if you would divine the future.

-Confucius

2

Background and Theory

ELEMENTS heavier than helium, or metals as they are referred to by astronomers, are one of the fundamental ingredients for planets to be able to take form. These heavy elements were not produced by the Big Bang or in the early Universe but are gradually made from fusion inside stars, being built up until released when the stars explode as supernovae. As time progress and more stars explode the Universe becomes more metal rich and we expect more planets to be able to form. A convenient way to estimate the metallicity content of a star is to measure its iron over hydrogen abundance and compare it to that of the Sun, so that $[\mathrm{Fe/H}] = \log_{10}(\mathrm{Fe/H})_{\mathrm{star}} - \log_{10}(\mathrm{Fe/H})_{\mathrm{Sun}} \approx \log_{10}\frac{Z}{Z_{\odot}}$.

By following the trend of star formation and supernovae feedback from an early Universe to now, one could be able to say something about the metal content of the Universe at different epochs. Since planet formation and metallicity is correlated one can also say something about the planet number density. Observations of both transit and radial velocity methods indicate that the presence of giant planets on close-in orbits around their host stars is strongly correlated with the metallicity of the star (FV05). Observations as well as simulations point to such occurrences to be incompatible with the existence of nearby low-mass planets (Armitage 2003; Latham et al. 2011). It may therefore appear as if, according to e.g. L01 to be a selection effect to where Earth-like planets may reside: too little metallicity and they are unable to form because of lack of material building blocks, too much metallicity and they get destroyed by the migration of much more massive planets. Thus, by finding the "sweet spot" for which Earth-like planets are most likely to orbit a star, we may predict how many of such planets have formed in the Universe since the Big Bang.

2.1 Previous work

In an earlier attempt to use metallicity as a quantity to estimate the age distribution of Earth-like planets, L01 composed the following 5-step process:

- Compare the metallicity distribution of stars in the solar neighbourhood and stars hosting hot Jupiters in order to obtain a probability of hosting hot Jupiters. This will then yield the probability of destroying Earth-like planets.
- Assume that the probability to produce Earth-like planets scales linearly with metallicity.
- Combine the probability to host a hot Jupiter and the probability to form Earth-like planets in order to estimate the probability of harbouring Earth-like planets as a function of metallicity.
- Apply current estimates of the star formation rate in the Universe and observations of high redshift metallicities to get the metallicity distribution of star-forming regions as a function of time.
- Combine the probability to harbour Earth-like planets as a function of metallicity with the metal distribution as a function of time to estimate the age distribution of Earth-like planets in the Universe.

In order to construct a metallicity dependent function for the probability to form a hot Jupiter, L01 applied observational Doppler data of 32 such host stars from Gonzalez (2000) and Butler et al. (2000). These host stars were compared to samples of Sun-like stars in the solar neighbourhood from Sommer-Larsen (1991) and Rocha-Pinto & Maciel (1996), to which L01 notes that the hot Jupiter hosts are significantly more metal-rich than the solar-neighbourhood star sample. The control sample of solar-neighbourhood Sun-like stars was not searched for planets with the Doppler technique and only served as a comparison to the metallicity distribution of Sun-like stars. Marcy & Butler (2000) found that out of $\sim$ 500 main sequence solar-type stars, 28 harbours giant planets on close in orbits, an average planet-finding efficiency to be 5.6%. Normalising this planet-finding efficiency so that the 32 host stars used by L01 represents 5.6%, that is, rescaling each bin of $N(\mathrm{Fe/H})$ so that $0.056 \sum_i N(\mathrm{Fe/H}) = 32$, L01 obtains the the histogram shown in Figure. 2.1. L01 assumes the mass fraction of metals in the Sun to be

$Z_\odot = 0.016$, so that the fraction of irons compared to hydrogen is Fe/H $\approx \log(Z/0.016)$.

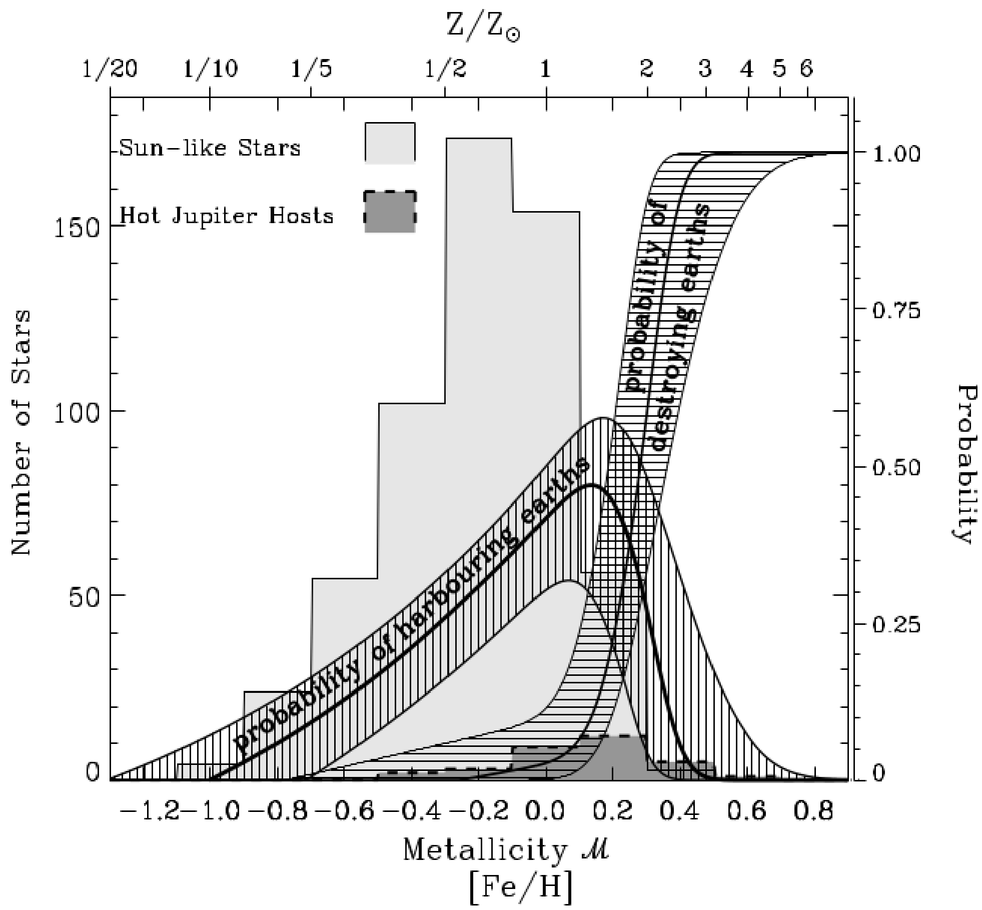

Figure 2.1: Sun-like stars in the solar neighbourhood that host Jupiter-sized planets (dark grey) are distributed towards higher metallicities compared to the mean of the total number of stars observed (light grey). If Jupiters preclude the existence of Earth-like planets in the same stellar system and assuming that the production of Earth-like planets is linearly proportional to the metallicity, we get the probability for stars to harbour Earth-like planets according to Equation 2.2. From Lineweaver (2001).

Also included in Figure 2.1 is the estimated relative probability that a star will host a hot Jupiter and thus probability of destroying Earth-like planets. For a given metallicity this is calculated by the ratio of number of stars hosting hot Jupiters and the number of stars targeted as

$$P_{\mathrm{DE}}(\mathrm{Fe/H}) = \frac{N_{HJ}(\mathrm{Fe/H})}{N(\mathrm{Fe/H})}. \tag{2.1}$$

For high metallicities, e.g. Fe/H > 0.4, this probability predicts that more than 95% of Sun-like stars will have Doppler-detectable hot Jupiters. The probability relation is very steep, going down to predicting 20% of stars hosting hot Jupiters at metallicities of Fe/H ~ 0.2 and dropping to $\sim 5\%$ at solar metallicity, Fe/H $= 0$. L01 argues that these predictions are supported by independent observations such as the detection of planet BD-10 3166 (Butler et al. 2000), which was found around a high metallicity star with Fe/H = 0.5, leading to a probability prediction of $P_{\rm DE}(\text{Fe/H}) \sim 1$. This star and planet detection were left out of the sample due to selection bias. The *Hubble Space Telescope* (HST) monitored the globular cluster Tucanae of thirty-four thousand stars with a mean metallicity of Fe/H = −0.7 for planet transits (Gilliland et al. 2000). No planets were found, a result consistent with the probability predicted by Equation 2.1 of $P_{\rm DE}(\text{Fe/H} = -0.7) \sim 0$. However, Gilliland et al. (2000) suggests that the lack of planets may be due to planetary stability being disrupted by the high stellar densities.

For the probability to form Earth-like planets, which L01 defines as planets within the mass range $0.5 < M/M_{\oplus} < 2$, a linearly increasing probability with increasing metallicity was assumed. Furthermore, the probability to form an Earth-like planet in the low metallicity regime of $P_{\rm PE}(\text{Fe/H} < -1.0)$ was set to zero. The probability was set to increase to its highest at the most metallic bin, Fe/H = 0.6, so that $P_{\rm PE}(\text{Fe/H} = 0.6) = 1$.

In order to calculate the probability of stellar systems harbouring Earth-like planets L01 simply multiplies the probability of producing Earth-like planets with the probability of not destroying them, or in other words, probability of not producing hot Jupiters.

$$P_{\rm HE}(\text{Fe/H}) = P_{\rm PE}(\text{Fe/H}) \times [1 - P_{\rm DE}(\text{Fe/H})] \tag{2.2}$$

The predicted probability of harbouring Earth-like planets is also plotted in Figure 2.1, increasing linearly from low metallicities, reaching its peak at Fe/H = 0.135, then gets cut off at Fe/H $\geqslant$ 0.3.

The star formation history of the Universe is very important and plays a dual role in this type of analysis. Both planet formation and metallicity build-up is directly proportional to the star formation rate (SFR). For the mean metallicity of star forming regions in the Universe, L01 assumes

$$\int_0^t \text{SFR}(t')dt' \sim \bar{Z}(t). \tag{2.3}$$

Since at any given time t, some star forming regions may have lower metallicity while some regions have higher metallicity, a time-dependent Gaussian dispersion was parametrised centred on the mean metallicity:

$$P(Z, \bar{Z}(t)) = \frac{1}{\sigma\sqrt{2\pi}} \exp\left[\frac{(Z - \bar{Z}(t))^2}{2\sigma^2}\right]. \tag{2.4}$$

To normalise this function, L01 assumes the mean metallicity value of OB stars derived by Gummersbach et al. (1998) as $Z/\bar{Z}_{\odot}(t_0) = 0.63$ for star forming regions today together with a dispersion of $\sigma = 0.3$. The fraction of stars being formed at a given time t that are capable of harbouring Earths is then estimated by the integral over metallicity as

$$f(t) \approx \int P(Z, \bar{Z}(t)) P_{\mathrm{HE}}(Z) dZ, \tag{2.5}$$

where $P_{\mathrm{HE}}(Z)$ is derived from Equation 2.2 and $P(Z, \bar{Z}(t))$ from Equation 2.4.

For the actual star formation history (SFH) of the Universe, L01 adopts results from Barger et al. (2000) with a peak in SFR at redshift $z \approx 5$. Furthermore, L01 restricts the attention to Sun-like stars in the mass range of $0.8 \leqslant M/M_{\odot} \leqslant 1.2$. It is then assumed that $\sim 5\%$ of the mass that forms stars form Sun-like stars within in the restricted mass range. The star formation rate as a function of time, SFR(t), can then be multiplied by a factor of $A \sim 0.05$ to yield the age distribution of Sun-like stars in the Universe.

By combining the fraction of Sun-like stars, probability to harbour Earth-like planets and SFR, an estimate for the Earth-like planet formation can be made for Sun-like stars as:

$$PFR(t) = A \times SFR(t) \times f(t). \tag{2.6}$$

When inserting the results from the integral of Equation 2.5 into Equation 2.6, one obtains not only an Earth-like planet formation rate for the Universe but also an age distribution of Earth-like planets orbiting Sun-like stars. L01 estimates this age distribution to have an average age of 6.4 ± 0.9 Gyr, i.e. ≈ 1.8 Gyr older than the current Earth.

Exactly what impact metallicity has for the formation of Earth-like planets is not fully understood, although a minimum threshold on the required metallicity for Earth-like planets to form seems obvious. Prantzos (2008; hereafter P08) utilises the same strategy as described by L01 above but assumes that stars have no metallicity dependency for the probability of forming Earth-like planets. Nevertheless, it has been empirically shown by e.g. FV05 that the occurrence rate of giant planets, *ergo* hot Jupiters, increases with increasing metallicity of the host star for FGK stars. Such correlation was also parametrised by FV05 as $P_{HJ} = 0.03(Z/Z_{\odot})^2$ which P08 adopts in order to estimate the probability for Earth-like planets to avoid being destroyed by hot Jupiters and survive. We further discuss the parametrising of the occurrence rates of planets in Section 3.1 and how it may influence our estimations.

2.2 Hot Jupiters & Planet Migration

Hot Jupiters are gas giant planets which are thought to have migrated from distances of several AUs to very short close-in orbits they are detected at. This subclass of planet is normally defined as planets with masses $M_p > 0.1M_J$ and periods $P < 10$ days. To understand the baseline for hot Jupiters better, we give a brief summary of the current theories for gas giant formation and planet migration in the following sections as well as their influences on the stellar-systems hosting them.

2.2.1 Giant Planet Formation

There are currently two recognisable scenarios which explain the formation of gas giant planets such as Jupiter and Saturn. The primary one, known as the *core accretion* model describes the process in which fragments of heavier elements which coagulate into planetesimals clump together to form a solid core. When this solid core grows massive enough and the escape velocity from its surface exceeds the thermal speed of the surrounding gas, a tenuous gas envelope will start to accumulate around its core (D'Angelo et al. 2010). A runaway gas accretion phase may occur if the pressure gradient within the envelope fails to balance the gravitational force, making the envelope contract and allow for more gas to be accreted. The amount of gas accreted is then determined by properties of the protoplanetary disk and governed by gravitational interactions between the disk and the protoplanet. Whilst embedded in the disk, the protoplanet will exert a gravitational torque on the gas which leads to an exchange of orbital angular momentum between the disk and the planet. Materials orbiting on the outside of the planet tend to gain angular momentum, thus moving towards larger radii, whereas angular momentum is lost for materials on the inside of the orbit of the planet, causing them to move towards even smaller radii. As the planet depletes the gas of the disk for each orbit, the process tends to create an annular gap in the local density distribution of the disk. A snapshot from a simulation of a migrating massive planet forming a gap is shown in Figure 2.2. The direction of the motion of the planet is then locked to the viscous evolution of the disk and will move together with the direction of the gas flow, which may cause an inward migration on the planet.

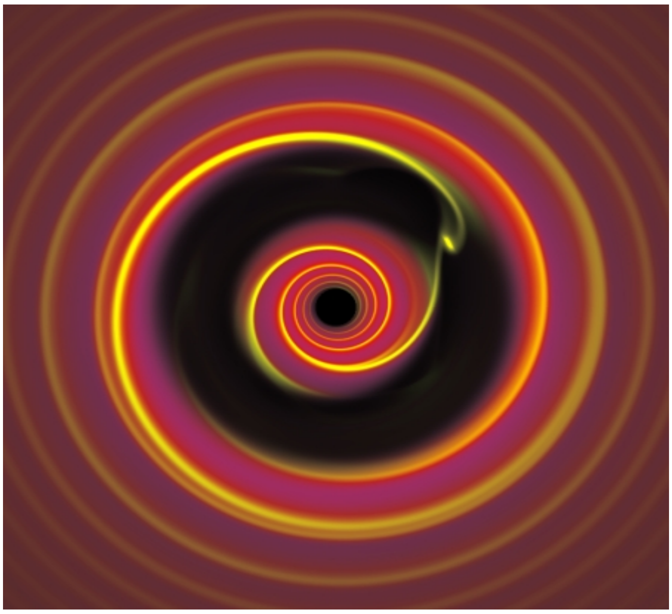

Figure 2.2: Snapshot from a simulation of a planet-disk interaction for "Type-II" migration in which a sufficiently massive planet opens up a gap in the gas disk. The massive planet is depicted by the yellow dot and the central star has been removed. A full movie showing the interaction as a function of mass is available at `http://jila.colorado.edu/~pja/planet_migration.html`. Courtesy of Armitage (2007).

The other scenario for giant planet to form is that they originate from *disk instabilities*. Much like stars that form through the gravitational collapse of interstellar clouds, it has been suggested by Boss (1997) that gas giant planets may form in similar ways. The theory proposes that through gravitational instabilities of a protoplanetary disk may lead to fragmentation of self-gravitating clumps. If conditions for disk instabilities prevail, planets may form directly out of the gas phase of the disk in a much shorter period of time compared to the core accretion model. Planets forming through the disk instability model gain most of their augmentation of gas immediately and gather planetesimals subsequently, which sediment to its heavy element core. One can differentiate the formation models as disk instability being top-down and initially rapid, whereas core accretion is initially slow and bottom-up.

Core accretion is favoured for high-metallicity systems where heavier elements are more abundant (e.g. Boss 2010). With an increased supply of heavier elements, more and heavier cores can be produced (e.g. Ida & Lin 2004). Spectroscopic Doppler surveys have shown an empirical correlation between host star metallicity and the occurrence of giant planets (e.g. FV05; Johnson et al. 2010). This strong correlation has often been taken as a strong argument for core accretion being the dominant and more prominent model for gas giant formation. Nevertheless, Doppler surveys are more sensitive to planets close to their host star and stronger spectral lines are shown in metal-rich stars, giving rise to a bias towards detecting massive planets on close-in orbits in metal-rich systems.

The disk instability model is still a good candidate to explain the observed giant planets orbiting very metal-poor stellar-systems such as HD 155358 and HD 47536, both of which have metallicities [Fe/H]$= -0.68$ (Cochran et al. 2007). It has also been suggested through simulations and theoretical work of e.g. Boley (2009) that disk instabilities may occur at very large radii where gas giant planets may form in situ. Due to the limitations on our current detection techniques, observational support for planets at very large orbits is scarce but this may improve in the future.

2.2.2 Planet Migration Influences

Gravitational interactions with the gaseous disk at the early stage of planet formation causing giant planets to migrate inwards, also known as "Type II"-migration (e.g. Ward 1997), is not the only way for planets to migrate and change their orbital periods. Planet-planet scattering for instance, causing a change in orbital period through loss or gain of angular momentum via ejection of other planets or planetesimals may occur long after the gas has dissipated from the disk (e.g. Chatterjee et al. 2008). Secular perturbations and orbital disruptions may also occur from interactions with distant binary companions by e.g. the *Kozai-Lidov mechanism* (Petrovich 2015).

Our earlier detections of hot Jupiters suggested that they are part of single-planet systems only, as they do not have companions on similar orbits (Ford 2014; Steffen et al. 2012). Results from *Kepler* transit photometry and Doppler radial velocity surveys show that low-mass planets on close-in orbits are extremely common around stars that do not host hot Jupiters (e.g. Bonfils et al. 2013; Fressin et al. 2013). The lack of observed low-mass planets around hot Jupiter hosts is often explained by the migration mechanism of the more massive planet being hazardous for the less massive planets (e.g. L01; P08). It is thought that the more massive planets interact with the less massive planets by, either ejecting them from the stellar system or colliding with them, destroying the low-mass planets in the process. Indeed, simulations by Mustill et al. (2015) show that high eccentricity migration of giant planets often destroys all low-mass planets on close-in orbits. The outcome may vary some, with some cases where the low-mass planets get destroyed by colliding with the star or ejected from the system. In some cases the giant planet accretes the low-mass planets and the core of the surviving giant planet gets enriched with heavy materials, which also increases the probability of it becoming a hot Jupiter. This latter case is supported by observations of giant planets on close-in orbits that have enriched cores such as H149026b (Wolf et al. 2007).

The knowledge of stars mass and metallicities may give clues to the role of planet migration in the observed population of exoplanets. Armitage & Rice (2005) argues that the correlation between giant planets and stars with high metallicity found by FV05 is not at all surprising. As the metallicity of the star increases, so does the surface density of planetesimals which in turn decreases the time scale for core accretion. They further argue that metallicity may well be the most prominent parameter, more so than gas disk mass and gas disk lifetime, in determining the probability of giant planet formation. With and increased amount of heavy elements there would also be more planetesimals to interact with post gas disk, leading to further interplay between giant planet and planetesimals.

Host star metallicity is undeniably a key factor in determining the outcome of a planetary system. N-body simulations by Cossou et al. (2014) for instance, show that high-metallicity systems have a much higher success rate for producing giant planet cores close to the host star, as well as multiple giant planet cores. Although the correlation between metallicity and giant planet formation they find is somewhat stronger than most observations, their finding is consistent with high-metallicity being a requirement for gas giants to form in multiple systems (Dawson & Murray-Clay 2013). Cossou et al. (2014) also find no correlation between metallicity and the occurrence of "super-Earths" (which they define as planets smaller than $1.5 - 2R_{\oplus}$), a result that is consistent with most observations (e.g. Buchhave et al. 2012). It has also been suggested by Benítez-Llambay et al. (2015) that increased metallicity, and thereby more solids and infalling material, can induce a heating torque which halts ongoing migration of giant planet cores. They argue that such mechanism could explain the pile-up of giant planets found orbiting high-metallicity stars whereas super-Earths have no need for enriched metallicities to form.

We can allow satellites, planets, suns, universe, nay whole systems of universes, to be governed by laws, but the smallest insect, we wish to be created at once by special act.

-Charles Darwin

3

Method & Procedure

In this section we describe our method used in this work and go into more detail on what data we use, what assumptions we make and how we acquire the results we get. Our first step is to define a means to describe the occurrences of planets without having to physically observe them. We propose a way to estimate the probability for a star of a certain mass and metallicity to host planets, a type of *planet occurrence recipe* one could say. Much like the strategy of L01 and P08, we assume smaller rocky planets to to be less abundant at very high metallicities where giant planets form instead. Before we go into detail on the ingredients in our recipe, we illustrate some different definitions of planets and disclose what goes into our estimations.

3.1 Planet Recipes

Both L01 and P08 prescribe their own recipes for the probability of stars to harbour Earth-like planets which we described in Section 2.1. Quite a lot has happened in the field of exoplanetary astronomy since then, e.g. the great success of *Kepler* has yielded over a thousand confirmed exoplanets[1] (Lissauer et al. 2014). We have much better means to make statistical estimates on the occurrence rates of planets orbiting stars today than ever before. We therefore produce our own estimates based on the occurrence rates of both low-mass planets and giants derived by recent transit and RV-surveys. In the following sections we give a more general description of the more recent works in the

[1] http://www.nasa.gov/kepler/discoveries

literature concerning occurrence rates and exoplanet surveys.

3.1.1 Planet Exposition

There are several ways to categorise observed exoplanets depending on their size and their mass. A common way to go about the classification of an exoplanet is to compare its features with those of planets in our Solar system, i.e. calling exoplanets with similar size or mass to that of Earth to be Earth-like and planets comparable to Jupiter to be Jupiter-like. Different literature may have other definitions of mass- and size limits as well as other names for the symbolism to Solar system planets. For instance, Buchhave et al. (2014) define three regimes of planet radii ranging from $< 1.7R_\oplus$ for Earth-like planets, $1.7 - 3.9R_\oplus$ for gas-dwarfs and $> 3.9R_\oplus$ for ice- and gas giants. Others may want to divide these regimes into several subgroups, e.g. Dressing & Charbonneau (2015; hereafter DC15) define Earth-like planets to have radii between $1 - 1.5R_\oplus$ and super-Earths to have $1.5 - 2.0R_\oplus$. Petigura et al. (2013) use *Kepler* data to determine the occurrence rate of terrestrial planets with radii $1 - 2R_\oplus$. These definitions can vary a lot depending on the method used to observe the planets with and the actual sample size. As *Kepler* utilises the transit method in order to detect exoplanets, it obtains information regarding the radius of the planet but no detail about its mass. Doppler, or radial velocity (RV) surveys on the other hand retrieve knowledge about the mass of the planet but not its radius.

In order to clarify the convention adopted here, we step away from the definition L01 makes of Earth-like planets being planets within the mass range $0.5 < M/M_\oplus < 2.0$ and select a broader variety of planets. We assign *terrestrial planets* to be of size $R_p \approx 0.5 - 2R_\oplus$, or have masses $M \approx 0.5 - 10M_\oplus$. Our definition may seem quite generous and includes both smaller rocky planets as well as what some literature defines as super-Earths. Nevertheless, by having a wider array of rocky-planets we obtain more stringent observational statistics for our purposes. Furthermore, when we use the notion *terrestrial planet* we refer to planets in the designated mass and size range and do not impose any special prospects on habitability.

We regard giants as planets more massive than $\gtrsim 30M_\oplus$ (or $\gtrsim 0.1M_J$) or with radii $R_p \gtrsim 3.9R_\oplus$. We also drop the "ice/gas" prefix to our definition of giant planets and only consider their actual size and mass, paying no attention to their composition. We do not consider planets between these two mass- and size regimes for our calculations, assuming that they do not affect the occurrence of terrestrial and giant planets. In our definition of giant planets we do not distinguish the subclass of hot Jupiters from our definition of giant planets. Our planet recipe consists of occurrence estimates for giant planets on small orbits < 2.5 AU, a territory where giant planets are seldom accompanied by terrestrial planets (e.g. Batygin & Laughlin 2015; Ford 2014; Latham et al. 2011).

Our definitions are argued for to be consistent with the observational data and the different metallicity-dependent power laws for the occurrence rate of giant planets, which we discuss in Sections 3.1.2 & 3.1.3 respectively.

Compilations of confirmed exoplanet populations can be obtained from e.g. `http://exoplanets.org/`. In Figures 3.1, 3.2, 3.3 & 3.4 we see plots of the confirmed exoplanets mass and radii plotted against their host star metallicity and mass. Although a trend between host star metallicity and planet size may be hinted from those plots, one has to keep in mind that these results are from different surveys of varying methods and that the observations are highly biased towards short orbits and massive planets. The differences in the number of exoplanets in each population is due to some planets not having well determined characteristics from their observed measurements.

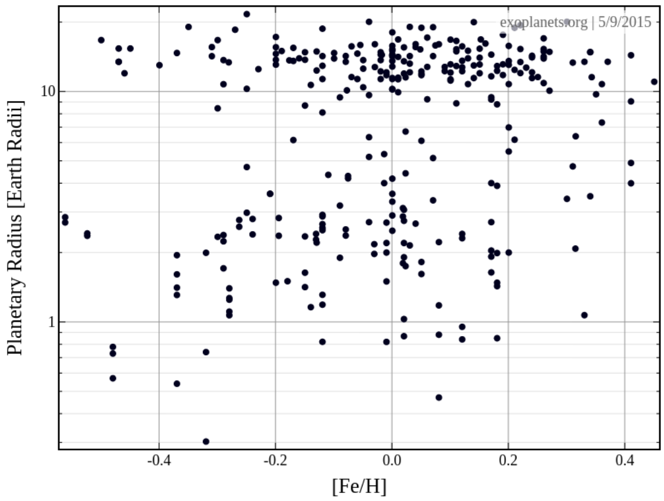

Figure 3.2: Exoplanet population plotted with planetary radii against host star metallicity. Courtesy of Han et al. (2014).

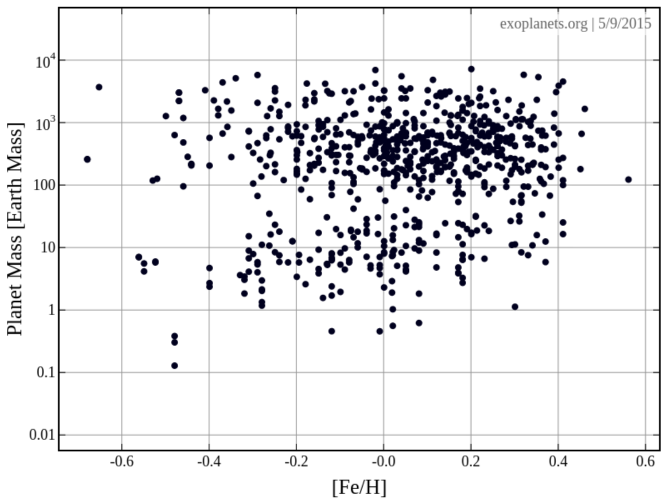

Figure 3.1: Exoplanet population plotted with planet mass against host star metallicity. Courtesy of Han et al. (2014).

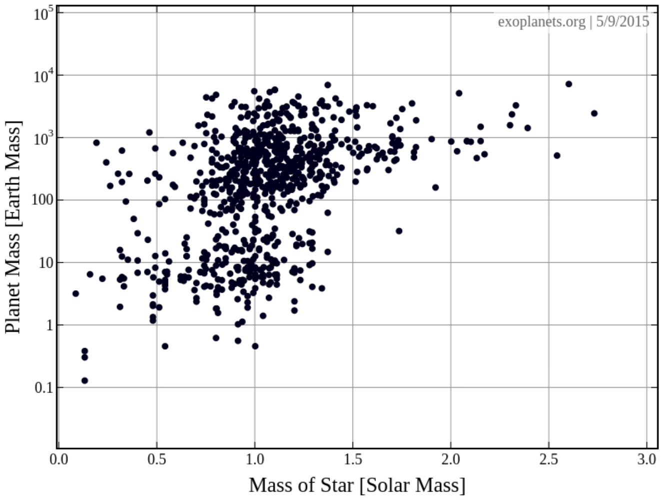

Figure 3.3: Exoplanet population plotted with planet mass against host star mass. Courtesy of Han et al. (2014).

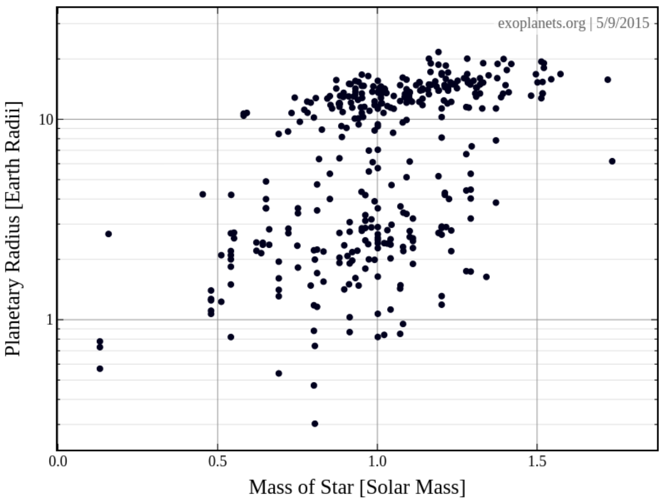

Figure 3.4: Exoplanet population plotted with planetary radii against host star mass. Courtesy of Han et al. (2014).

A vast majority of stars are thought to form in multiple systems (e.g. Kroupa 2002), yet most exoplanets are observed orbiting single stars (e.g. Mullally et al. 2015). This may be due to an observational effect as eclipsing binaries can sometimes dilute the observations and masquerade as a planet detection (e.g. Petigura et al. 2013). Planets belonging to binary star systems have been confirmed (e.g. Doyle et al. 2011), although most of these detections are to be considered as giant planets to our definition ($M_p \geqslant 0.1 M_J$). Simulations have shown the circumbinary environment to be friendly to planet formation and that one should expect terrestrial planets to join the growing demographics of circumbinary planets (Bromley & Kenyon 2015). In our work we assume planet formation to be the same for single as well as for binary stars, something that does not necessarily have to be the case. We also assume that all stars have the same probability to harbour planets at a given stellar mass and metallicity.

3.1.2 Occurrence Rates

The earlier work by L01 and P08 considered only solar- and similar to solar type stars to harbour terrestrial planets. Their samples of stellar populations constituted FGK spectral type stars with masses ranging from $0.8 - 1.2\ M_{\odot}$. Later observations have shown that less massive stars may also harbour Earth-sized planets. As it turns out, according to e.g. Dressing & Charbonneau (2013; herafter DC13); Mulders et al. (2015) and more, the occurrence rate of smaller sized planets is higher around low mass M-dwarfs than for more massive stars. Swift et al. (2013) argue that terrestrial planets orbiting M-dwarfs may be as much as twice as abundant compared to G-dwarfs and occurs three times more frequent than for F-type stars. We present parts of several occurrence rate estimates from different surveys in Table 3.1, some of which are used in later calculations.

The definitions of exoplanet class may differ for each reference in Table 3.1. For instance, Fressin et al. (2013) defines giant planets as planets with radii $> 6R_{\oplus}$, implying that their occurrence rate for our definition of giants with radii $> 3.9R_{\oplus}$ becomes too low when attached to our definition. Our definition of the regimes for terrestrial- and giant planets is quite generous and enclose all other regimes for the tabulated values presented here. Therefore we can see the values in Table 3.1 as lower limits on the occurrence rates within our planet mass and size regimes.

Table 3.1: Samples of occurrence rates of number of planets per star from the literature that we make use of in our calculations. The full range of occurrence rates for different planetary radii, mass, period and host star types can be seen within the respective reference. We display the orbital period in days which corresponds the orbital radius presented in some of the literature.

Reference	Method	Spectral type	Period (days)	Planet type	Occurrence
Bonfils et al.	Doppler	M-dwarfs	1-100	$1 - 10M_{\oplus}$	0.710
Bonfils et al.	Doppler	M-dwarfs	< 100	$100 - 1000M_{\oplus}$	0.030
Cassan et al.	μ-lens	KM-dwarfs	$\sim 10^2 - 10^4$	$5 - 10M_{\oplus}$	0.62
Cassan et al.	μ-lens	KM-dwarfs	$\sim 10^2 - 10^4$	$100 - 3000M_{\oplus}$	0.17
DC13	Transit	M-dwarfs	<50	$0.5 - 1.4R_{\oplus}$	0.51
DC15	Transit	M-dwarfs	<100	$1.0 - 1.5R_{\oplus}$	0.678
DC15	Transit	M-dwarfs	<100	$1.5 - 2.0R_{\oplus}$	0.608
Fressin et al.	Transit	Sun-like	< 85	$0.8 - 1.25R_{\oplus}$	0.184
Fressin et al.	Transit	Sun-like	< 85	$1.25 - 2.0R_{\oplus}$	0.230
Fressin et al.	Transit	Sun-like	< 418	$6 - 22R_{\oplus}$	0.052
Howard et al.	Transit	Sun-like	< 50	$8 - 32R_{\oplus}$	0.013
Petigura et al.	Transit	Sun-like	<100	$1 - 2R_{\oplus}$	0.262
Petigura et al.	Transit	Sun-like	<100	$4 - 16R_{\oplus}$	0.045
Tuomi et al.	Doppler	M-dwarfs	1-100	$3 - 10M_{\oplus}$	1.08

The occurrence rates tabulated in Table 3.1 have some discrepancy between the two observational modes. Others have also pointed this out and Wang et al. (2015a) identify the estimated occurrence rate for hot Jupiters to be a factor of 2-3 smaller for transit surveys compared to Doppler. This difference could be explained by Doppler surveys systematically targeting stars with higher metallicity as they give rise to stronger spectral lines (Lovis & Fischer 2010). Another plausible reason for the difference could be that transit surveys may misidentify hot Jupiters as smaller planets by being subjects to photometric dilution and contamination of subgiant stars. Wang et al. (2015a) investigates this probability to find that 12.48% of hot Jupiters are misidentified by *Kepler* and advise that the estimated occurrence rate of hot Jupiters by *Kepler* surveys should be revised upwards.

Kepler mission surveys that utilise the transit method in order to detect exoplanets suffer greatly from the difficulty of detecting planets on large orbits. With increasing orbital period around its host star, a planet has an increased chance of being aligned in such way that it goes unnoticed by our observations. Petigura et al. (2013) took *Kepler* data of Sun-like stars and estimated an occurrence rate of planets with radii $R = 1 - 2R_{\oplus}$ on periodical orbits less than 100 days to be increasing linearly with the logarithm of the period. This linear relation is shown in Figure 3.5, obtained from Petigura et al. (2013), where they proceed to extrapolate the occurrence rate up to higher orbits. For our planet occurrence recipe we assume the occurrence of terrestrial planets to be 0.4 planets per FGK-star. This occurrence rate is based on the extrapolated value to $P \sim 400$ days by Petigura et al. (2013) with a generous adaptation to account for smaller planets.

3.1.3 Mass-Metallicity Correlation

Both simulations and observations suggest that giant planets are more bountiful at metal-enriched environments and the list for supporting a correlation between stellar host metallicity and the occurrence rate of giant planets grows ever longer (e.g. Armitage & Rice 2005; Johnson et al. 2010). Buchhave et al. (2014) analysed more than 2000 high-resolution spectra of *Kepler* Objects of Interest (KOI), yielding parameters of 405 stars orbited by 600 exoplanet candidates. In their survey, they placed planets into three regimes depending on the planet sizes; small rocky planets with $R < 1.7R_{\oplus}$, gaseous dwarfs with radii $1.7 < R/R_{\oplus} < 3.9$ and giant planets with $R > 3.9R_{\oplus}$. They examine the metallicity of the host stars of these planet regimes and find that the median metallicity for smaller planets is sub-solar whereas giant planet hosts have a median metallicity of ~ 1.5 times that of the Sun.

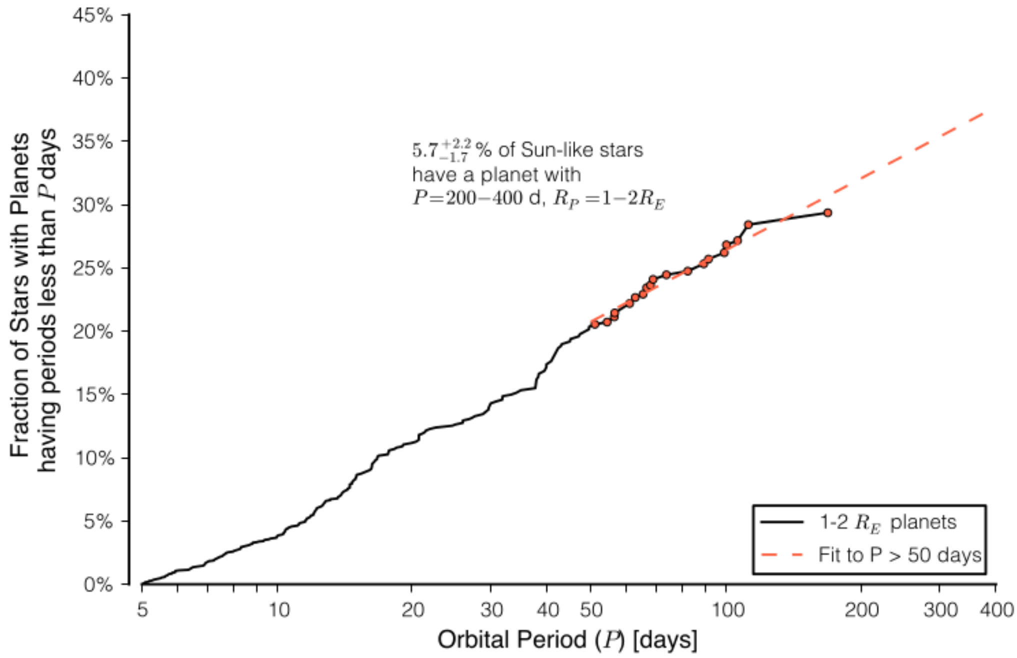

Figure 3.5: Fraction of stars having nearly Earth-sized planets ($1-2R_\oplus$) with any orbital period up to a maximum period P. The cumulative distribution of planet occurrences reaches 20.4% at $P = 50$ d, in other words, 20.4% of Sun-like stars harbour a $1-2$ $R_\oplus$ planet with an orbital period $P < 50$ d. The linear increase in this cumulative quantity corresponds to planet occurrence that is constant in equal intervals of log$P$. Modest extrapolation to $P = 400$ days yield that $\sim 5.7\%$ of Sun-like stars host planets of size $1-2$ $R_\oplus$ with orbital period of $P = 200-400$ days. Courtesy of Petigura et al. (2013)

With increasing evidence for a metallicity-correlation, FV05 proposed that the occurrence rate of Jupiter-sized giant planets orbiting FGK-type stars can be described by a simple power law on the form[2]

$$f_{\text{Giants}}(\text{Fe/H}) = f_0 10^{a[\text{Fe/H}]} \tag{3.1}$$

FV05 found the parameters to be $f_0 = 0.03$ and $a = 2$, which we have compile together with other literature results in Table 3.2. The metallicity recipes of Neves et al. (2013) contains two cases, one for the HARPS sample only and one for a combination of both the HARPS M-dwarf sample and the CPS M-dwarf sample.

It has also been suggested by e.g. Johnson et al. (2010); Montet et al. (2014) that the occurrence rate of giant planets increases monotonously with increased stellar mass. Mulders et al. (2015) argue for a stellar mass drop in occurrence rates, suggesting that giant planet formation and migration rates increase with stellar host mass. Clanton & Gaudi (2014) estimates that the occurrence rate of giant planets (they define giant

[2] Same power law as we discussed in Section 2.1.

planets to be in the mass range $50 < M/M_{\oplus} < 10^4$) orbiting M-dwarfs is a factor of 2.2 smaller than for FGK-type stars. In combination with the metallicity correlation of Equation 3.1, they propose a mass-metallicity power law function on the form

$$f_{\text{Giants}}([\text{Fe/H}], M_*) = f_0 10^{a[\text{Fe/H}]} M_*^b, \tag{3.2}$$

where $M_* = M/M_{\odot}$. Values derived from the literature to fit the parameters in the power law function are presented in Table 3.3.

We plot these power laws against a range of metallicities from $-0.5 \leqslant [\text{Fe/H}] \leqslant +0.5$ in Figure 3.6. Some of these power laws are derived from samples of stars with more or less reserved boundaries of metallicities and mass. For instance, the power law of FV05 is argued to be valid in the metallicity range in the figure but most of the stars in the sample used by Montet et al. (2014) had metallicities in the range $-0.6 <$ [Fe/H] $< +0.2$. Nevertheless, we apply these power laws describing the occurrence rate of giant planets to our calculations, bearing in mind that they may not very well represent the population outside their designated mass- and metallicity range.

We note that there is quite a huge difference in the estimation of the a parameter between Neves et al. (2013) and GM14 for M-dwarfs. From Table 3.2 we gather that the estimation of $a = 1.06$ by GM14 is much lower than both the HARPS ($a = 1.97$) and the combined HARPS & CPS sample ($a = 2.94$) found by Neves et al. (2013). GM14 also point out this discrepancy and make an attempt to explain why this is. By substituting some of the stars in their sample for the Neves et al. (2013) HARPS sample they calculate a similar power law parameter of $a = 1.99$, suggesting that the fault lies not

Table 3.2: Metallicity power law parameters for Equation 3.1.

Reference	Spectral type	f_0	a
Fischer & Valenti	FGK	0.03	2
Neves et al. HARPS	M	0.02 ± 0.02	1.97 ± 1.25
Neves et al. Comb.[3]	M	0.03 ± 0.02	2.94 ± 1.03

Table 3.3: Mass-metallicity power law parameters for Equation 3.2.

Reference	Spectral type	f_0	a	b
Gaidos & Mann	FGK	0.070	1.80 ± 0.31	~ 1
Gaidos & Mann	M	0.070	1.06 ± 0.42	~ 1
Montet et al.	M	$0.039^{+0.056}_{-0.028}$	3.8 ± 1.2	$0.8^{+1.1}_{-0.9}$
Johnson et al.	FGKM	0.07 ± 0.01	1.2 ± 0.2	1.0 ± 0.3

[3]Combined sample of HARPS and CPS M-dwarfs.

in the methodology. The most likely explanation is that the difference comes from the exact distribution of metallicities in the samples themselves. Another important issue to consider is the very steep power law, depicted by the green line in Figure 3.6 (Montet et al. 2014), which shows a greater occurrence rate for giant planets orbiting M-dwarfs than most of the FGK-type power laws (e.g. FV05; GM14). The reason behind this steep power law with $a = 3.8$ is most likely due to the sample itself and the definition of giant planets by Montet et al. (2014). By only considering planets of Jupiter mass and above, Montet et al. (2014) exclude a $0.7M_{\text{Jupiter}}$ massive planet with a rather metal-poor host, [Fe/H]$= -0.19$, which Neves et al. (2013) include in their estimate of the shallower power law of $a = 2.94$. It would appear that the small sample sizes of M-dwarf giant planet hosts make the power laws very sensitive to outliers from the expected trend and that the inclusion of a single additional planet can change the slope of the power law drastically.

Another difference that may affect the estimated power laws is the orbital periods of the detected planets in the different surveys. Most RV surveys include only orbital periods of less than 4 years, (e.g. FV05 and Johnson et al. 2010 restrain orbits to $P < 2.5$ AU and GM14 to $P < 2$ years) making such surveys incomplete for longer periods. One way to go about the limited range of orbital periods detectable by RV surveys is to include data from microlensing surveys, which Montet et al. (2014) do and extrapolate the occurrence rate for periods up to $P \leqslant 20$ AU. Some concerns about including microlensing to RV surveys that Clanton & Gaudi (2014) explore is that the targeted stars can vary quite a bit. Distant M-dwarfs near the Galactic bulge targeted by microlensing surveys may have a very different metallicity distribution compared to nearby M-dwarfs targeted by RV-surveys.

3.1.4 Probability to Harbour Terrestrial Planets

In the estimation on the probability to form an Earth-like planet, L01 assumed a gradually increasing probability with increasing metallicity of the host star. One would expect the necessity of a minimum metallicity for a star in order to host a terrestrial planet, but a well defined trend of a large number of terrestrial planets at higher metallicities remains unobserved. L01 further explains that one reason for this may be due to the observed trend of increased occurrence rate of giant planet hosts at higher metallicities. Giant planets that formed at several AU may due to interactions with the gaseous protoplanetary disk and loss of angular momentum migrate inwards towards the host star. The migration of a massive giant planet destroys the disk and any smaller planets in

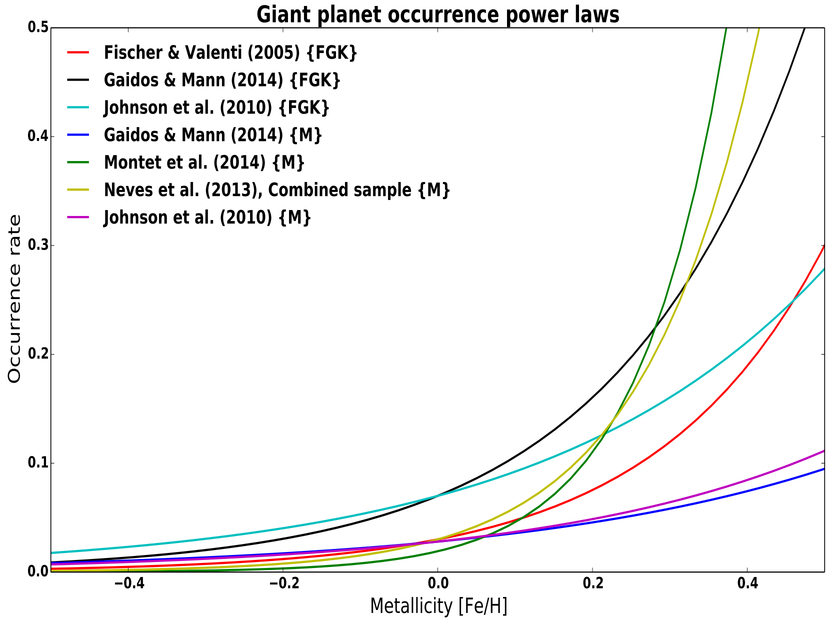

Figure 3.6: Occurrence rate of giant planets described by power laws of Equations 3.1 & 3.2 and parameters from Tables 3.2 & 3.3. Parameters for M-dwarfs are evaluated at a mass of 0.4 $M_\odot$ and FGK types at 1 $M_\odot$. Note how the occurrence rate described by Montet et al. (2014) (green line) for M-dwarfs differs from other M-dwarf giant host metallicity recipes. This is most likely an effect from the definition of a "giant" planet where Montet et al. (2014) limit their sample to planets more massive than 1 Jupiter. The black and blue lines of Gaidos & Mann (2014) represent the power law for forming giant planets adopted in our planet occurrence recipe for harbouring terrestrial planets. A plot in log-scale of the occurrence rate is shown in Figure 3.7.

its path. Gravitational scattering interactions between planets are also only favourable for the more massive planets, likely to eject the less massive planets from the stellar system. It is therefore argued by L01 and P08 likely that at higher metallicities when giant planets have a higher probability to be formed, the probability of them being a hazard for and destroying terrestrial planets during their migration phase increases as well.

For our planet recipe we impose the occurrence rate of terrestrial planets harbouring FGK-stars to be $f_{p,\mathrm{FGK}} = 0.40$. This value is based on the value Petigura et al. (2013) find for the occurrence rate of planets of size $R = 1 - 2R_\oplus$, extrapolated to orbits $P < 400$ days for *Kepler* FGK-stars. We further assume the occurrence rate of planets orbiting M-dwarfs to be $f_{p,\mathrm{M}} = 1$. That most, if not all M-dwarf stars host low-mass planets with $R = 0.5 - 2.0R_\oplus$ seems to be the consensus of both *Kepler* transit and Doppler RV surveys (e.g. DC15; Bonfils et al. 2013; Tuomi et al. 2014). For our estimation of the probability for stars to form giant planets that impede the possibility

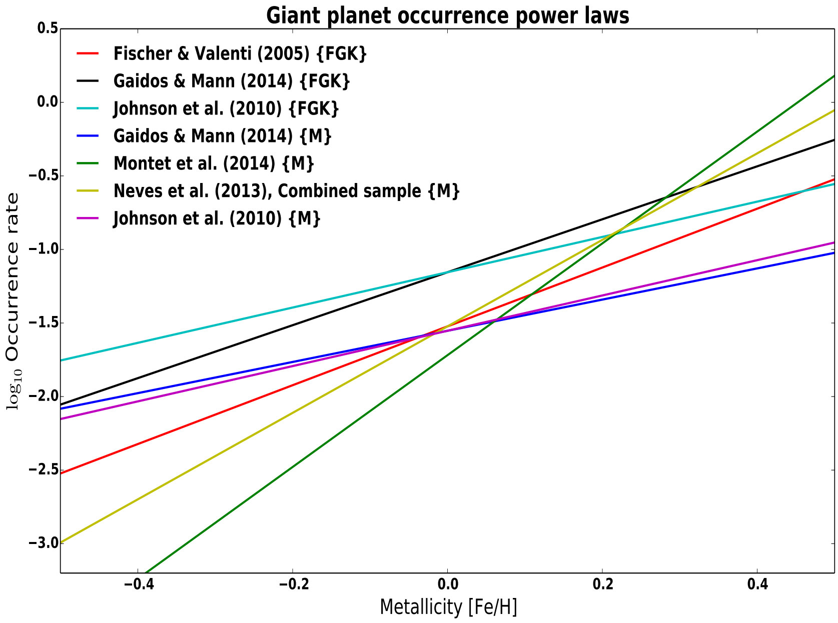

Figure 3.7: Same as Figure 3.6 with log scale on occurrence rates for a more detailed view at the low-metallicity ends of the power laws. Some of the power laws were not derived for the metallicity range plotted here and may not be very well represented. Power laws with additional mass-correlation are evaluated with $M = 0.4M_{\odot}$ for M-dwarfs and $M = 1.0M_{\odot}$ for FGK-stars.

for low-mass planets to inhabit the stellar-system we apply the power laws derived by GM14. We assign M-dwarfs to be of mass $0.08 - 0.6M_{\odot}$ and FGK-stars to be of mass $0.6 - 1.2M_{\odot}$. This choice of definition is made in order to attempt to be consistent with the surveys our parameters are obtained from. The evolution of our planet occurrence recipe and those of L01 and P08 as functions of metallicity is portrayed in Figure 3.8.

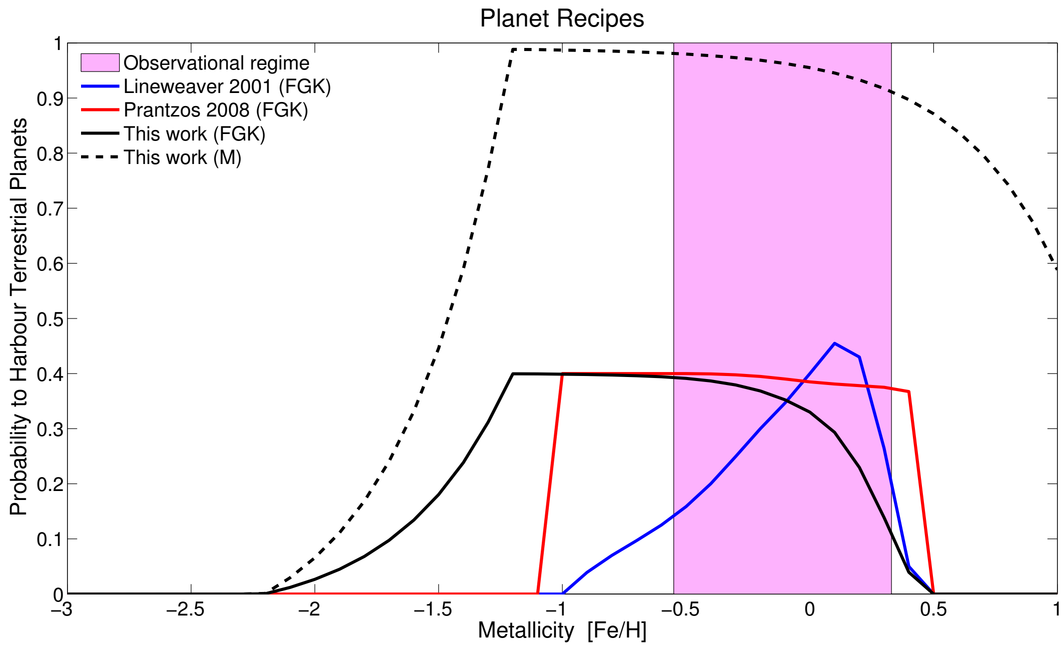

Figure 3.8: Probability for harbouring terrestrial planets according to different planet occurrence recipes. The blue line depicts the metallicity relation derived by Lineweaver (2001) and the red line the relation used by Prantzos (2008). The black solid line represents our planet recipe where we assumed the occurrence rate of terrestrial planets of $\leqslant 0.4$ in accordance with the result of Petigura et al. (2013) and apply the occurrence rate of giant planets to match the power law of Gaidos & Mann (2014). The black dashed line is the probability for M-dwarfs to host terrestrial planets for our planet occurrence recipe, where the adopted occurrence rate for terrestrial planets to be $\leqslant 1$ according to the results of *Kepler* (e.g. Dressing & Charbonneau 2015) and RV-studies (e.g. Tuomi et al. 2014). The rose-tinted area describes the regime to which where have actual observations of terrestrial planets.

The planet occurrence recipe is calculated from the occurrence rates described above, with a gradually increasing probability to form terrestrial planets from [Fe/H]$\geqslant -2.2$ to its maximum occurrence at [Fe/H]≈ -1.2. The probability to form terrestrial planets is then assumed to be constant and flat towards higher metallicities. We then apply the power law for estimating the occurrence of giant planets on short orbits and subtract it from the terrestrial planet occurrence rate in order to estimate how many stars will harbour terrestrial planets. A comparison of our planet occurrence recipe and the already existing works of L01 and P08 is preformed and the result is shown in Table 4.1.

3.2 The Semi-Analytic Model

Our method of estimating the number of terrestrial planets in the observable Universe requires insight on the cosmic star formation history (SFH) and chemical evolution from a very young Universe until this very day. A good way to obtain these quantities is to apply simulations of galaxy formation over a large volume and length of time. Because the process of galaxy formation involves a wide variety of physical processes and non-linear physics, the task of simulating galaxy formation is far from trivial. The two main paths to bypass this issue are N-body/hydro-dynamic (smooth particles) simulations, a technique that attempts to numerically solve the physical processes inherent to galaxy formation; and semi-analytic modelling, a technique that constructs a coherent set of analytic approximations which to describe the same physics.

Because N-body/hydro-dynamical methods attempts to solve the nonlinear physics behind galaxy formation directly they can be more accurate in some aspects. On the other hand, they are quite expensive computationally whereas semi-analytic models make good use of approximations which facilitates the inclusion of more kinds of physical processes and bigger samples of galaxies (Henriques et al. 2009). The two different simulation techniques have shown good consistency on scales much larger than their resolution limits with restricted physical properties and for individual galaxies (e.g. Helly et al. 2003; Stringer et al. 2010). As we are mostly interested in the SFH and chemical evolution of many galaxies over large volumes, the semi-analytic model seems like a good choice of method to go with. A more general description of how the semi-analytic models used here work is given in Section 3.2.1.

For the purposes of this project we make use of **GALFORM**[4] (Cole et al. 2000) from the Durham semi-analytic model group and the open source **Galacticus**[5] (Benson 2011) semi-analytic models. We will refer to them as the Durham- and Galacticus models and give a comparison of the two different models in Section 3.2.2 and the different results they yield in Section 4.

3.2.1 Theory

The semi-analytic models presented here apply a hierarchical galaxy formation approach which is based on a *cold dark matter Universe*-model (ΛCDM). By taking the results of state of the art N-body simulations such as the Virgo Consortium Millenium Simulation (Springel et al. 2005), one obtains structures of the cosmic web. These structures are based on the cosmology applied to the simulations where initial fluctuations are randomly distributed and density patterns follow through gravitational instabilities. Snapshots from a simulation showing the time evolution of such density patterns formed by

[4] `http://icc.dur.ac.uk/index.php?content=Research/Topics/O8`

[5] `https://sites.google.com/site/galacticusmodel/`

dark matter haloes can be seen in Figure 3.9. These dark matter haloes are the cradles of hierarchical galaxy formation which requires knowledge on the abundance of such haloes, their masses, angular momentum and their formation history. The assembly of dark matter haloes can be extracted from the N-body simulations in the form of *merger trees*, where the haloes can be identified by some percolation algorithm, e.g. friends-of-friends. A schematic illustration of a merger tree for a dark matter halo is shown in Figure 3.10.

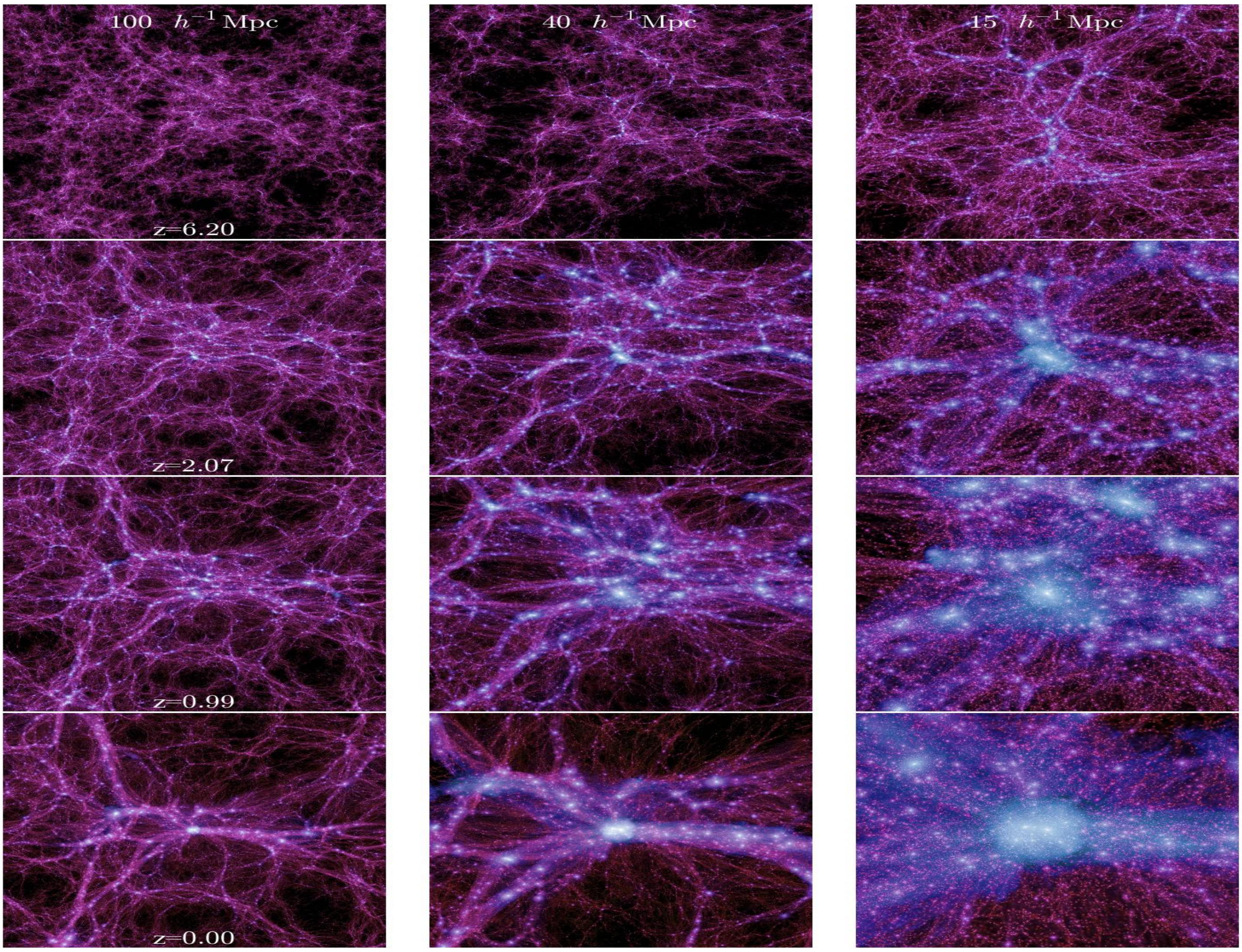

Figure 3.9: Time evolution of the formation of a massive halo from the Millennium-II Simulation. From left to right: 100, 40 and 15 Mpc/h in comoving units. From top to bottom $z = 6$, 2, 1 and 0. Courtesy of Boylan-Kolchin et al. (2009)

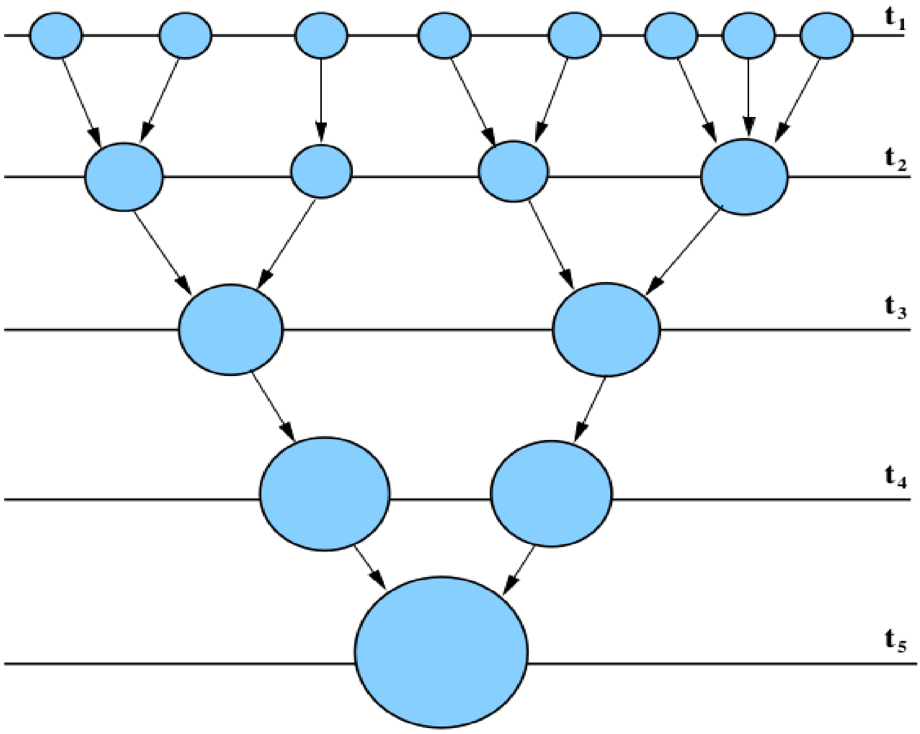

Figure 3.10: Schematic of a dark matter halo merger tree. Horizontal lines represent timestamps of snapshots in the evolution of the history of the halo, corresponding to the N-body simulation or Monte-Carlo realisation of the merger tree. The mass of the halo is depicted by the size of the circle, which grows through merger events between haloes and by accretion of objects below the halo mass resolution. The final halo is shown at t_5. Courtesy of Baugh (2006).

With dark matter haloes in place, one can assign other physical properties to them such as a gas cooling, star formation, supernovae and galaxy mergers. These properties are implemented differently depending on the semi-analytic model and are continually being improved and developed further. A simple overview of the typical processes incorporated into semi-analytic models is shown Figure 3.11. Semi-analytic models are at the mercy of our current understanding of the physical properties implemented into them as well as the quality of the underlying simulation. For a more in-depth description of semi-analytic models we refer the reader to the review on hierarchical galaxy formation by Baugh (2006).

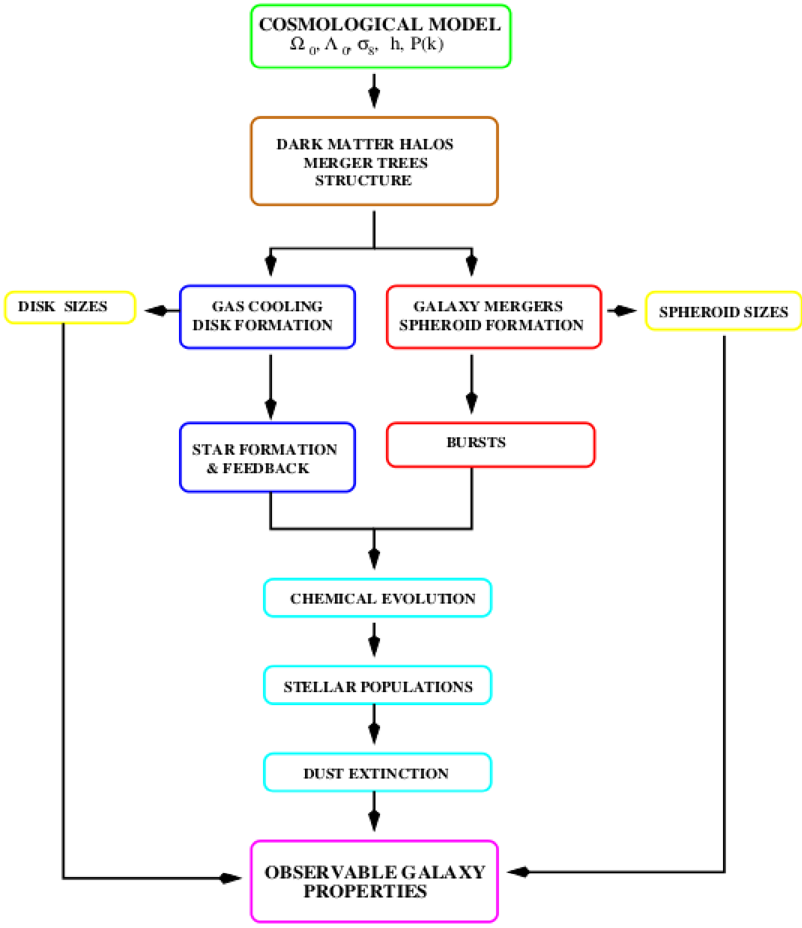

Figure 3.11: A schematic overview of the different ingredients and processes involved of a hierarchical galaxy formation model. Figure originally from Cole et al. (2000) and later adapted by Baugh (2006).

3.2.2 Model Data Comparion

The models at our disposal extracted data from simulated galaxies in comoving volumes of size $(64/h)^3$ and $(62.5/h)^3$ respectively for the Durham and the Galacticus model, where $h = 0.73$ km s^{-1} Mpc^{-1}. From our models we obtained the following quantities from the evolution of galaxies in their respective comoving volume:

Stellar mass: Each galaxy was composed of star particles of different masses. This was true for both of our models, although the resolution of the Durham model was limited to galaxies and star particles $M > 10^6 M_\odot$.

Stellar age: Each stellar particle had its own age from the time it formed. According to the cosmology used here, the Universe is 13.46 Gyrs old and the youngest stars born at redshift $z = 0.0$ were formed at that time. The oldest stars from our models were formed at redshift $z = 10.073$, corresponding to an age of the Universe as ≈ 0.46 Gyr.

Stellar metallicity: Each stellar particle also had a metallicity content. In the Galacticus model the metallicity of the stellar particles was ranging between a lower and an upper value of predetermined metallicity bins. The bins were chosen to give a good enough resolution to match our planet recipe (see Section 3.1.4) with values ranging between $-2.2 \leqslant [\mathrm{Fe/H}] \leqslant +1.0$ with steps of 0.2 dex. In addition to those metallicity bins a lower limit of 0 and upper limit were added to signify metallicities outside our range which did not contribute to our planet estimations. We randomly distributed the metallicity value between the lower and upper bin for each stellar particle in order to assign its metallicity and apply the lower and upper bin values as uncertainties.

Disk/Spheroid part: Each stellar particle was either part of the disk or the spheroidal component of the galaxy. For the Galacticus model we designated galaxies with more than half of its mass as disk components to be *disk dominated* and vice versa for *spheroid dominated* galaxies. For the Durham model we did not have masses of the disk/spheroidal parts but instead assumed galaxies with greater scale heights of the disk to be disk dominated and galaxies with greater bulge scale heights to be spheroidal dominated.

We compare the data of two models at redshifts, $z = 0.0, 0.5$ & 2.0, corresponding to lookback times of $t_{\mathrm{lookback}} \approx 0, 5$ & 10 Gyrs. We chose these three redshifts as they represent the Universe at very different times during a long portion of its entirety.

Both our models predict a similar amount of ≈ 36000 galaxies in their respective comoving volume at redshift $z = 0.0$. However, the properties of these galaxies were quite different for each model in terms of mass, age and metallicity distributions. The difference in mass of the galaxies at redshift $z = 0.0$ can be seen in Figure 3.12. The Galacticus model clearly predicts three distinct mass-regimes for its galaxy population as low-mass between $M_{\mathrm{Gal}} \lesssim 10^7 M_\odot$, intermediate mass for $10^7 M_\odot \lesssim M_{\mathrm{Gal}} \lesssim 10^{10} M_\odot$ and high-mass for $M_{\mathrm{Gal}} \gtrsim 10^{10} M_\odot$. The Durham model on the other hand predicts a smoother distribution of masses for galaxies, centred at $\sim 10^9 M_\odot$. The reason that the Durham model does not predict any galaxies of masses $< 10^7 M_\odot$ is due to the limitation of its resolution. In total, the Galacticus model predicts ~ 4.5 times the mass of the Durham model, most of which comes from the high-mass regime. The trend of different mass-regimes in the Galacticus model and higher total mass is also seen at higher redshifts, seen in Figures 3.13 & 3.14. In Figure 3.14 we plotted the mass distribution at redshift $z = 2.0$ and make note of the mass difference between the two models being somewhat higher, with Galacticus predicting ~ 5.7 times the more total stellar mass than the Durham model.

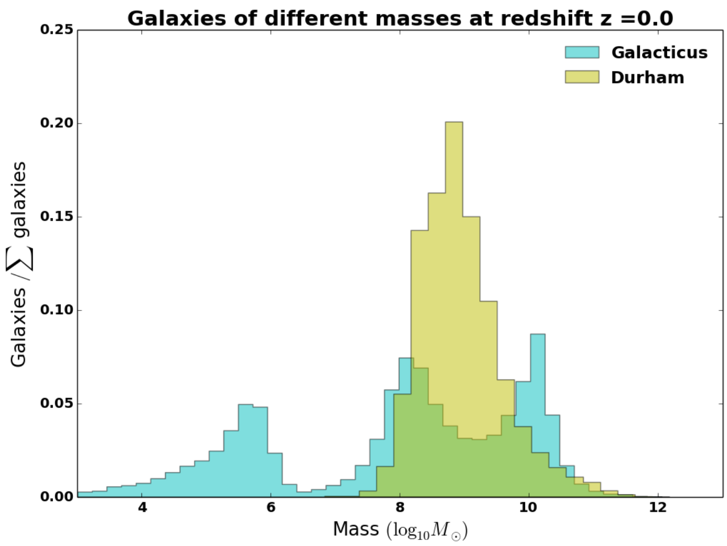

Figure 3.12: Mass distribution of galaxies at redshift $z = 0$ predicted by our semi-analytic models. The Durham model predicted a total number of $N_{\text{Gal}} = 35816$ galaxies whereas Galacticus predicted $N_{\text{Gal}} = 35657$. The light blue bars represent the Galacticus model and the yellow bars the Durham model. The histogram bars are transparent, so that bars overlapping the same mass-bins will appear green.

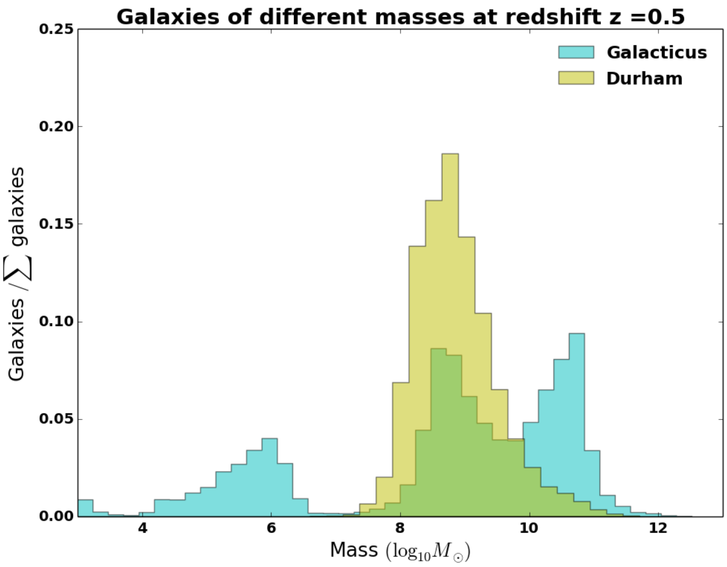

Figure 3.13: Mass distribution of galaxies at redshift $z = 0.5$ predicted by our semi-analytic models. The Durham model predicted a total number of $N_{\text{Gal}} = 36803$ galaxies whereas Galacticus predicted $N_{\text{Gal}} = 39255$. The histogram bars are transparent, so that bars overlapping the same mass-bins will appear green.

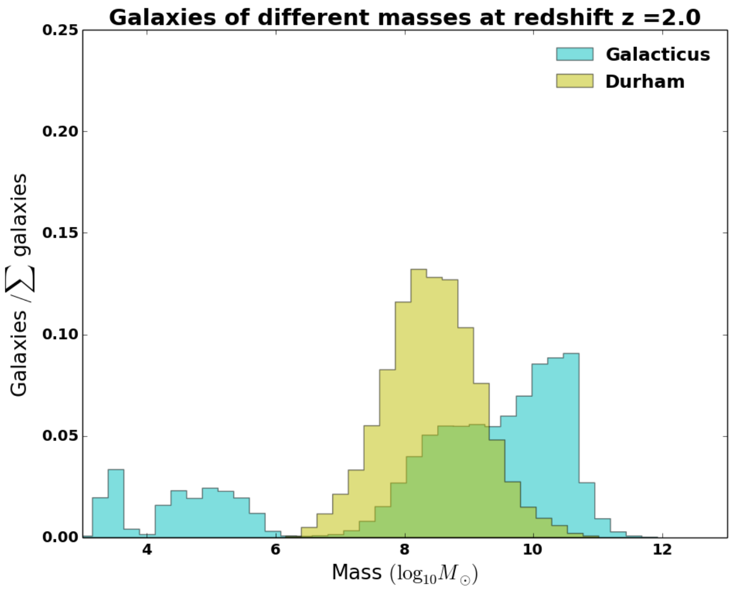

Figure 3.14: Mass distribution of galaxies at redshift $z = 2$ predicted by our semi-analytic models. The Durham model predicted a total number of $N_{\mathrm{Gal}} = 36767$ galaxies whereas Galacticus predicted $N_{\mathrm{Gal}} = 43836$. The histogram bars are transparent, so that bars overlapping the same mass-bins will appear green.

Not only is the mass distribution of galaxies very different for the models but the metallicity distribution as well. In Figures 3.15 & 3.16 we plot the mass-weighted mean metallicity against the mass of the galaxies for both models at redshift $z = 0$. We also estimate a mean value for the mean-metallicity for galaxies in mass-bins of size $\Delta \log_{10} 10^{0.5}$, displayed by the red dots in the figure. Both models predict higher metallicity towards galaxies of higher mass, which appears reasonable as massive galaxies may have undergone merger-events that triggered starbursts, thus creating more stellar mass and higher rate of supernovae to distribute heavy elements later on. The Durham model does not entail anything about galaxies $< 10^7 M_\odot$ but the Galacticus model predicts these galaxies to be very metal deficient. On the other hand, the Durham model predicts very few galaxies with super-solar metallicity whereas the Galacticus model anticipates almost all galaxies $> 10^{10} M_\odot$ ($\sim$ a third of all galaxies) to have more than two times the solar metallicity.

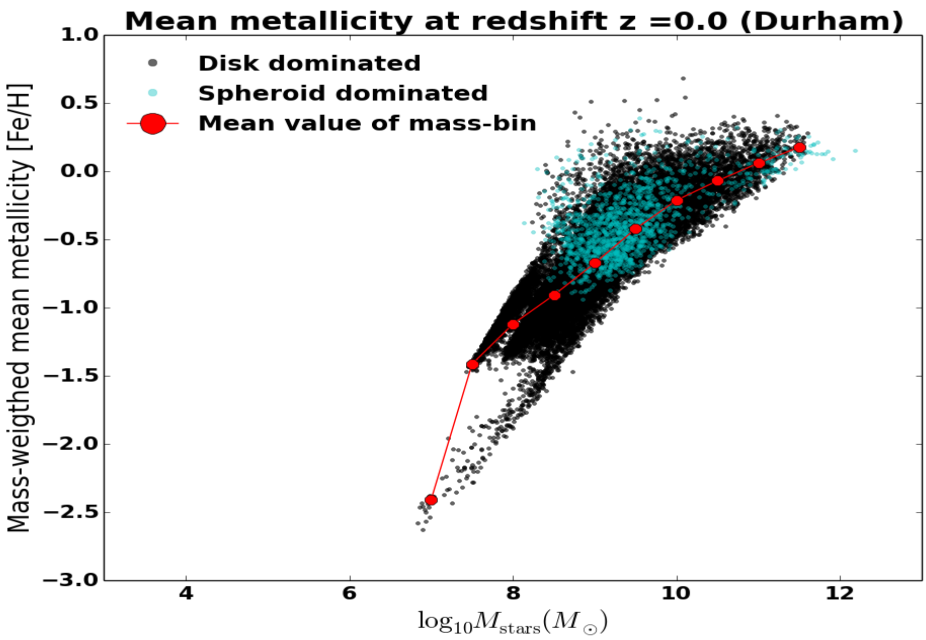

Figure 3.15: Mean-metallicity distribution of galaxies in the Durham semi-analytic model. The black dots represents disk-dominated galaxies, the cyan dots spheroid-dominated galaxies and the red line with dots is the mass-weighted mean value of each mass-bin of size 0.5 dex. The model predicts 34471 ($\approx$ 96%) disk-dominated and 1345 ($\approx$ 4%) spheroid-dominated galaxies.

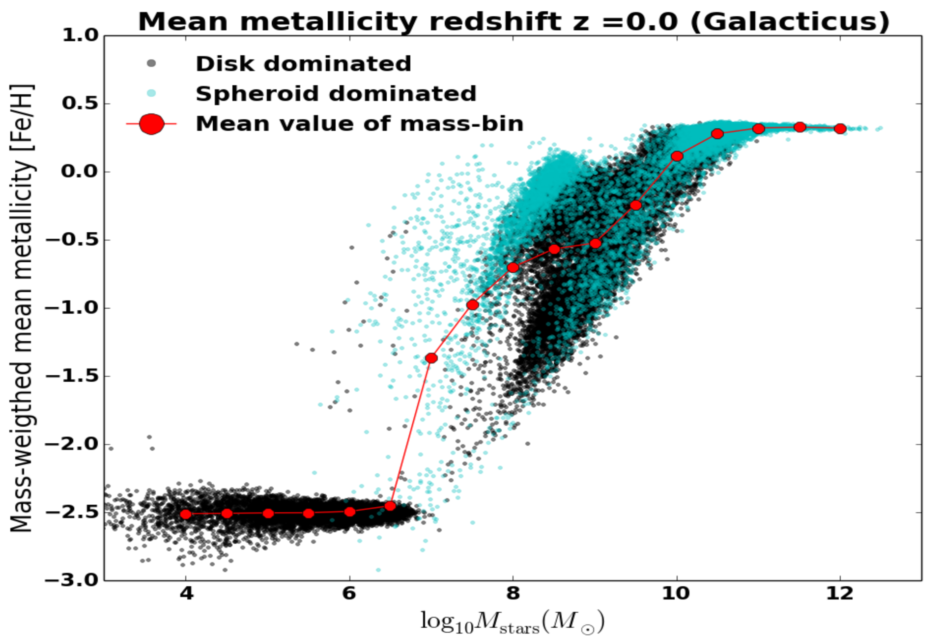

Figure 3.16: Mean-metallicity distribution of galaxies in the Galacticus semi-analytic model. The black dots represents disk-dominated galaxies, the cyan dots spheroid-dominated galaxies and the red line with dots is the mass-weighted mean value of each mass-bin of size 0.5 dex. The model predicts 23599 ($\approx$ 66%) disk-dominated and 12058 ($\approx$ 33%) spheroid-dominated galaxies.

The evolution of the metallicity predicted by the models and show that the Galacticus model has developed galaxies with high metallicity already at redshift $z = 2$. In Figures 3.17 & 3.18 we show the mass-weighted mean metallicity distribution of galaxies at redshifts $z = 0.0, 0.5$ & 2.0 for the Durham and the Galacticus model respectively. The Durham model shows a distribution of metallicities centred upon a mean value that increases over time. The inclusion of low-mass galaxies in the Galacticus model gives rise to the low-metallicity spike seen to the left in Figure 3.18.

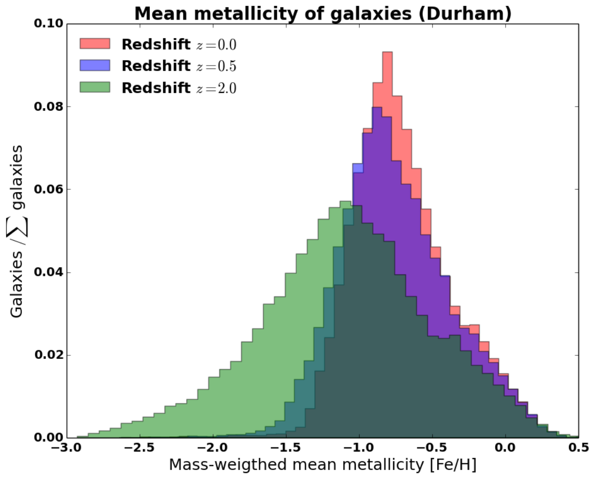

Figure 3.17: Mean-metallicity evolution of galaxies predicted by the Durham semi-analytic model for redshift $z = 0.0, 0.5$ and 2.0, corresponding to lookback times $t_{\text{lookback}} \approx 0, 5$ and 10 Gyr. The redshifts $z = 0.0, 0.5$, and 2 are plotted as histograms of colours red, blue and green respectively. The histogram bars are transparent, so that overlapping bars in the same metallicity bin may appear in a different colour. The histograms are normalised to the total number of galaxies at each redshift.

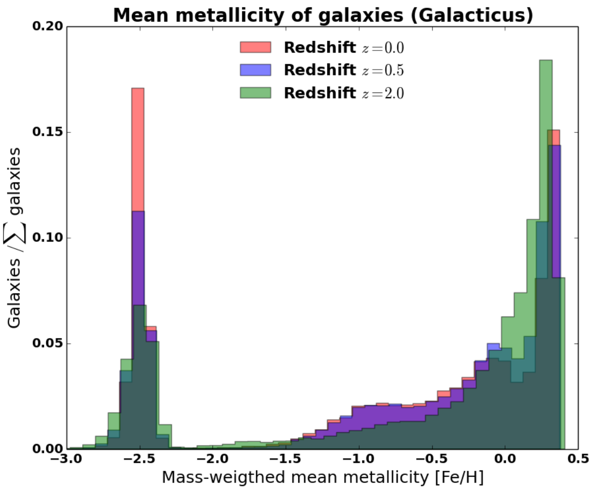

Figure 3.18: Mean-metallicity evolution of galaxies predicted by the Galacticus semi-analytic model for redshift $z = 0.0, 0.5$ and 2.0, corresponding to lookback times $t_{\text{lookback}} \approx 0, 5$ and 10 Gyr. The redshifts $z = 0.0, 0.5$, and 2 are plotted as histograms of colours red, blue and green respectively. The histogram bars are transparent, so that overlapping bars in the same metallicity bin may appear in a different colour. The histograms are normalised to the total number of galaxies at each redshift.

We also compare the mass-weighted mean stellar age of the galaxies predicted by the models, shown in Figures 3.19 & 3.20 where we again include a mean value of the mean-age in mass-bins of size 0.5 dex. The Durham model predicts a mean age of galaxies in the mass range of $10^8 - 10^{10} M_\odot$ to be ≈ 8 Gyrs whereas Galacticus shows a great increase in mean age for increasing stellar mass of the galaxies. We also see from Figure 3.20 that most low-mass galaxies are disk-dominated and that spheroid-dominated galaxies tend to be more massive and old.

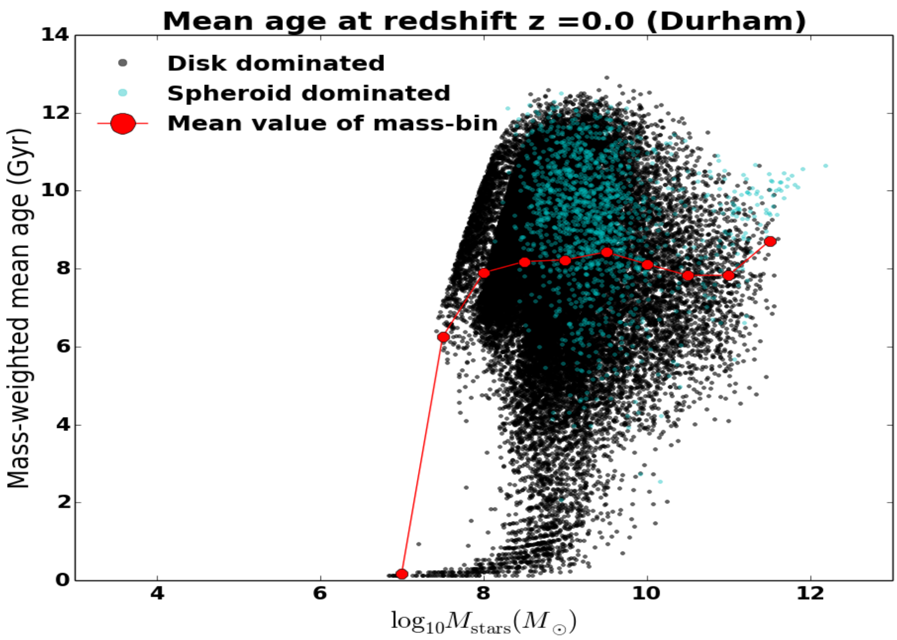

Figure 3.19: Mean-age distribution of galaxies in the Durham semi-analytic model. The black dots represents disk-dominated galaxies, the cyan dots spheroid-dominated galaxies and the red line with dots is the mass-weighted mean value of each mass-bin of size 0.5 dex. The model predicts 34471 ($\approx$ 96%) disk-dominated and 1345 ($\approx$ 4%) spheroid-dominated galaxies.

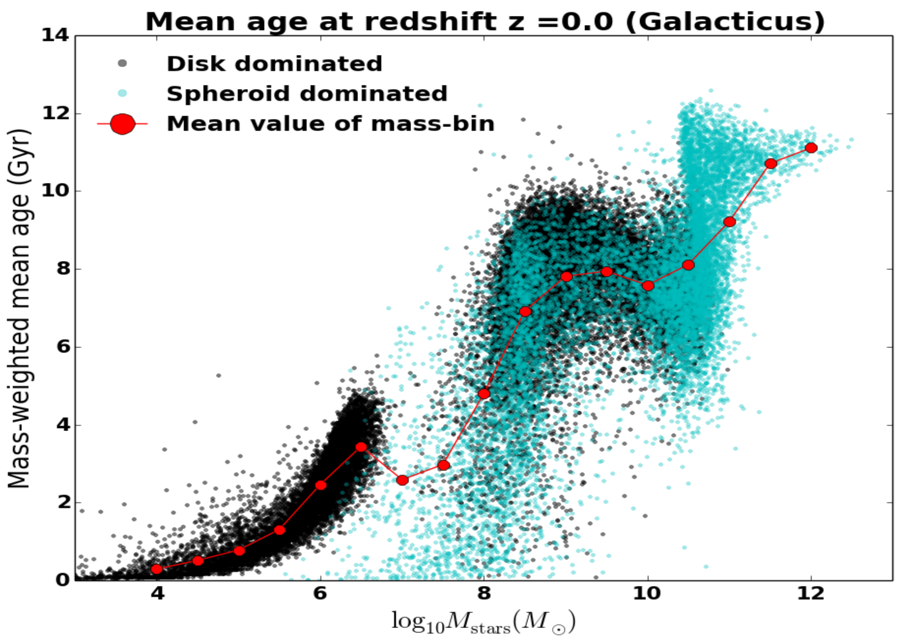

Figure 3.20: Mean-age distribution of galaxies in the Galacticus semi-analytic model. The black dots represents disk-dominated galaxies, the cyan dots spheroid-dominated galaxies and the red line with dots is the mass-weighted mean value of each mass-bin of size 0.5 dex. The model predicts 23599 ($\approx$ 66%) disk-dominated and 12058 ($\approx$ 33%) spheroid-dominated galaxies.

3.2.3 Literature Comparison

When we compare the raw data from our semi-analytic models with each other we note that they disagree on several points. We can further examine the star formation rate (SFR) of the models and compare them to that of observations. Ultraviolet (UV) continuum emission is dominated by short-lived massive stars in all but the oldest galaxies. Thus with a given stellar initial mass function (IMF), UV-observations can be used a direct measure of the SFR. Galaxies with extremely high SFR (i.e. starburst galaxies) tend to be filled with dust which absorbs UV light and re-radiates it in the thermal infrared (IR) (Sparke & Gallagher 2007). Such radiation can therefore be used as a sensitive tracer for young stellar populations and the cosmic star formation history (SFH). Madau & Dickinson (2014) compiled recent UV- and IR-observations of star formation rates at redshifts up to $z \approx 8$ and 4 respectively and estimates a best-fit function for the cosmic SFH as a function of redshift as

$$SFR(z) = 0.015\frac{(1+z)^{2.7}}{1+[(1+z)/2.9]^{5.6}}. \tag{3.3}$$

We calculate the SFR from our semi-analytic models by adding up the mass that formed at different times and divide it by the time difference between that and next interval. The Galacticus model has a slightly different cosmology, with parameters $(\Omega_M, \Omega_\Lambda, h) = (0.25, 0.75, 0.73)$ which we adjust for when we calculate the SFR of the model. Our semi-analytic models only provide us with stars up to redshift $z \approx 10$, which we plot together with Equation 3.3 in Figure 3.21. In the figure we also include a sample of the observational measurements compiled by Hopkins (2004); Lanzetta et al. (2002); Madau & Dickinson (2014), depicted by the different symbols. We restrict the observational data to a small selected sample in in the figure just to visualise the trends of the observations. We also include a plot of the SFH as a function of lookback time instead of redshift in which we exclude the observational data points, seen in Figure 3.22. We further extrapolate the SFR from our models to redshift $z = 20$ where we assume the first stars to have been formed (Visbal et al. 2012).

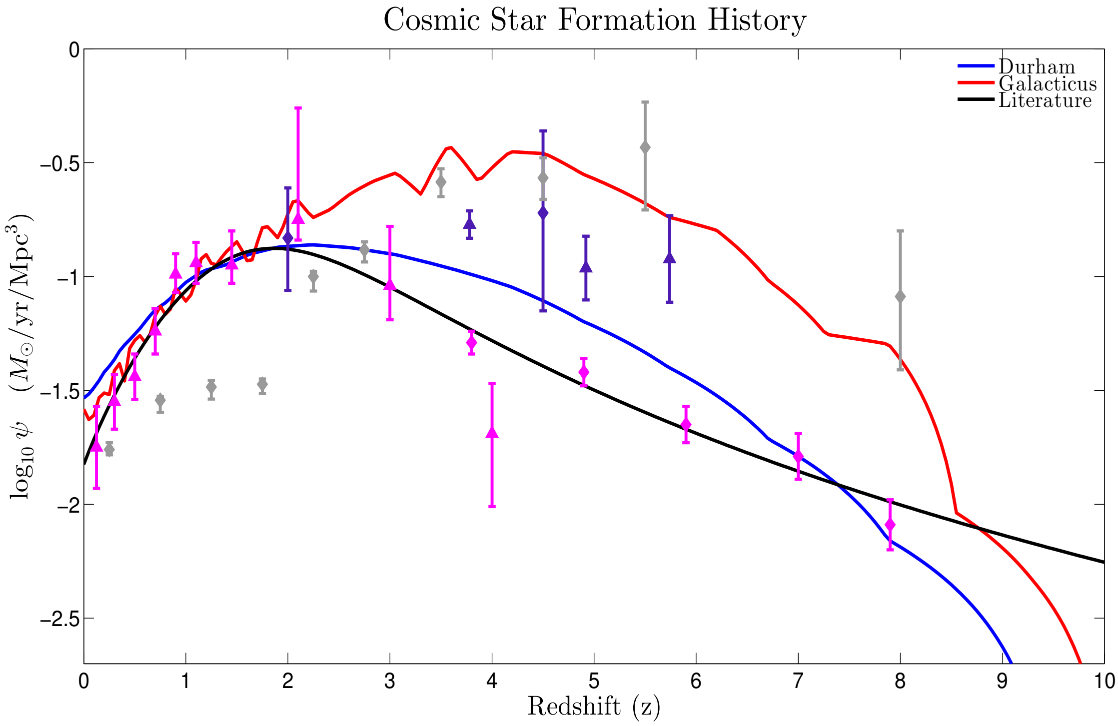

Figure 3.21: Cosmic star formation history. The blue and red lines show our semi-analytic models calculated SFR in solar masses per comoving Mpc^3 and the black line is the fitted function of Equation 3.3 (Madau & Dickinson 2014). The data points with symbols represent observational data with errors from the literature as following: The gray diamonds represent observational data from Lanzetta et al. (2002), the purple markers compiled results from Barger et al. (2000) (diamonds) and Giavalisco et al. (2004) (triangles) by Hopkins (2004). The magenta markers are results compiled by Madau & Dickinson (2014) obtained from Bouwens et al. (2012a,b) (diamonds) and Cucciati et al. (2012) (triangles). Errors in redshift is excluded in the figure to avoid cluttering. At redshift $z \gtrsim 10$ the SFR flattens out to steeply decline at redshift $z \approx 20$ where we assume the first stars to be formed.

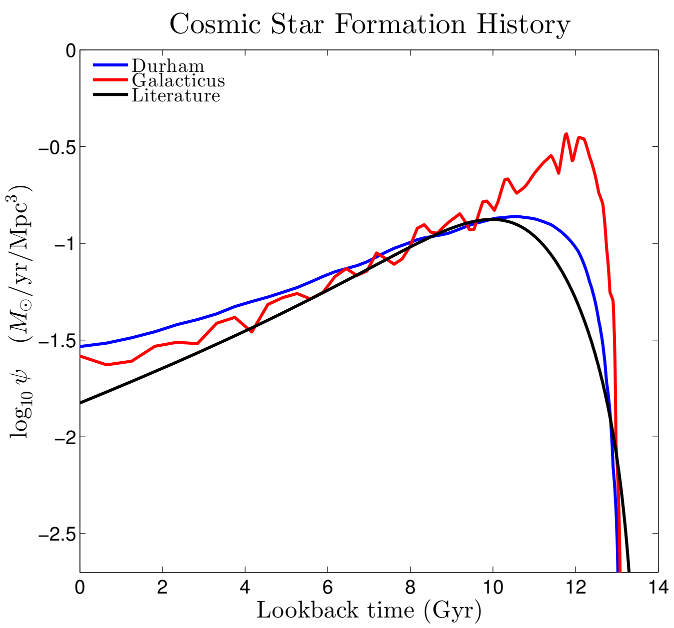

Figure 3.22: Cosmic star formation history as a function of time. The blue and red lines show our semi-analytic models calculated SFR in solar masses per comoving Mpc^3 and the black line is the fitted function of Equation 3.3 (Madau & Dickinson 2014). Here we can clearly see that the Galacticus model predicts a higher SFR in the early history of the Universe. At later times the Galacticus SFR has subdued to become lower than that of the Durham model, yet still higher than the that of the literature. This will later have some impact on the estimated typical age of stars predicted by the models, see Section 4.2.

Compared to the literature value of the SFH, our models overestimate the star formation rate at redshifts betwixt $2 \lesssim z \lesssim 8$. Nevertheless, the SFH up to redshift $z \lesssim 2$ is fairly consistent amongst both models and the literature, which corresponds to the longest time interval in the history of the Universe ($t_{\mathrm{lookback}}(z = 2) \approx 10$ Gyrs). We should point out that even though the SFR estimated by the Galacticus model, indicated by the black line in Figure 3.21, is much higher than both the Durham model and the literature value, it is still within observational error measurements (e.g. Hopkins 2004; Hopkins & Beacom 2006; Lanzetta et al. 2002). From the SFH we could estimate the stellar density per comoving volume and Mpc^3 at different redshifts, which we plotted in Figure 3.23.

The star formation rate at different epochs may be obtained from the measured luminosities of high-redshift galaxies, but obtaining estimates for metallicities is not as straightforward and usually requires spectroscopic measurements to be well constrained (e.g. Kewley & Ellison 2008). Nevertheless, a simple function of redshift for the metallicity content of stellar populations in the redshift range of $0 \lesssim z \lesssim 3$ was derived by Kewley & Kobulnicky (2007) as

$$Z_* = Z_\odot 10^{-0.15z}. \tag{3.4}$$

It should be noted that this relation is not very well constrained and should be taken as an illustrative measure of the metallicity only. It does however, fit well with the local Universe metallicity survey of Gallazzi et al. (2008) who find the metallicity at the local Universe to be $\sim 1.04 Z_\odot$. We plotted the mass-weighted mean metallicity of our models and Equation 3.4 over redshifts $z = 0 - 10$ in Figure 3.24. Note that for the chemical evolution we calculate the mass-weighted mean metallicity of the stellar particles from the semi-analytic models. The more massive galaxies as well as more massive stellar particles have high metallicity. In other words, the mass-weighted mean value is greater than the most common bin in Figures 3.17 & 3.18 where we plotted the mean metallicity of galaxies normalised to the total number of galaxies.

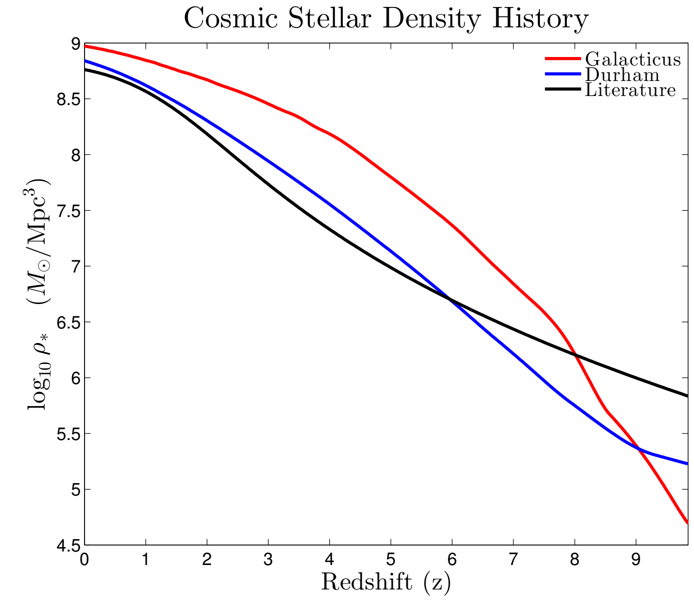

Figure 3.23: Stellar density in logarithm of solar masses per comoving volume and Mpc^3. The blue and red lines show the stellar density at given redshifts estimated by our semi-analytic models and the black line shows the literature value described by Equation 3.3 from Madau & Dickinson (2014).

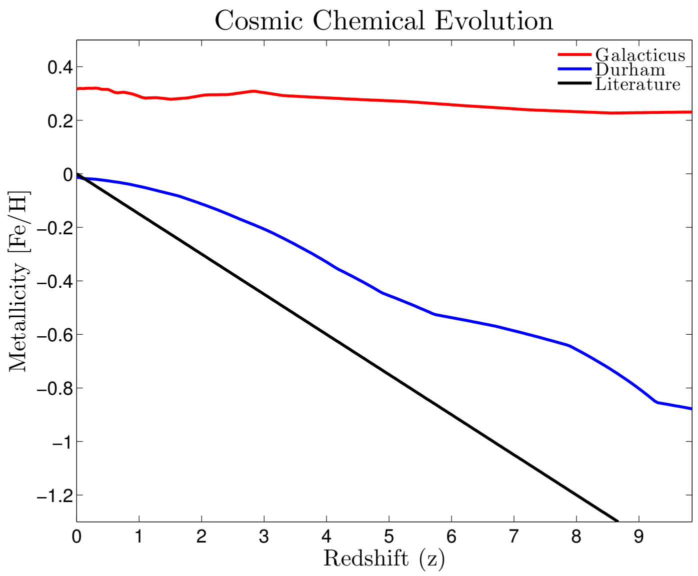

Figure 3.24: Cosmic chemical evolution. The blue and red lines show our semi-analytic models estimated mass-weighted mean metallicity of the newborn stellar population in logarithm of solar units, [Fe/H]. The black line display the metallicity of newborn stars according to Equation 3.4 derived by Kewley & Kobulnicky (2007).

A difference in a much greater mass-weighted mean metallicity is evidently shown in Figure 3.24 for the Galacticus model. This could be because of the very massive galaxies predicted by the model are also metal-rich, skewing the mean value upwards. These many differences displayed by the semi-analytic models and the literature will show their marks when we apply our planet recipe, which is discussed in Section 4. The metallicities obtained from our models at low redshifts are fairly consistent with the findings of observational surveys by Gallazzi et al. (2008) and simulations by Nagamine et al. (2001), suggesting that most metals are locked up in high-massive galaxies with older stellar populations.

3.3 Data processing

In this section we go into a bit more detail on some of the calculations we made regarding the initial mass function, metallicity distribution from our models and how we deal with short-lived stars.

From the cosmic SFH we calculate the expected stellar mass per comoving volume per Mpc^3 to form at redshifts $z = 0 - 20$ with a resolution of $\Delta z = 0.05$. In order to convert the stellar density ρ_* into total stellar mass in the sky, we calculate the concentric comoving volume up to said redshifts and slice it into bins of same redshift resolution. We do this by subtracting the inner concentric comoving volume from the outer comoving volume in said steps of $\Delta z = 0.05$. The stellar density per comoving volume and Mpc^3 is shown in Figure 3.23 and the slices of comoving volumes is plotted in Figure 3.25. The comoving volume is calculated using the cosmology calculator of Wright (2006)[6] with the cosmology adopted here.

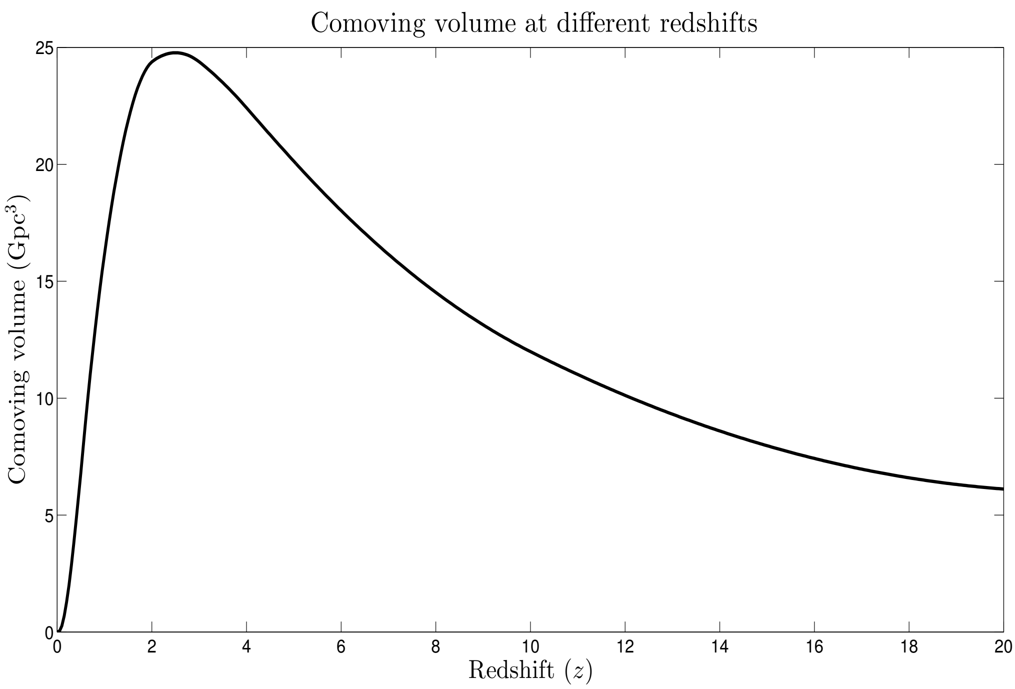

Figure 3.25: Concentric comoving volume in slices of $\Delta z = 0.05$ of the entire sky. Calculated from the cosmology calculator by Wright (2006).

[6] http://www.astro.ucla.edu/~wright/CosmoCalc.html

3.3.1 Initial Mass Function

An empirical function that describes the distribution of initial masses for a population of stars is often referred to as the *initial mass function* (IMF). The number of stars in a specific mass range from a given mass of a stellar population is evaluated by

$$\xi(M) = \xi_0 \int_{M_l}^{M_u} M^{-\alpha} dM \tag{3.5}$$

where ξ_0 is a normalisation constant, the limits M_l and M_u are the lower and upper boundaries to which stellar masses one is interested in and α is the power law index. For our calculations we assume the revised IMF derived by Kroupa (2001), but we acknowledge that there are several other choices such as the log-normal IMF of Chabrier (2003). The Kroupa IMF can be described by a broken power law as

$$\alpha = \begin{cases} 0.3 & \text{if} \quad 0.01 < M_* < 0.08 \\ 1.8 & \text{if} \quad 0.08 < M_* < 0.5 \\ 2.7 & \text{if} \quad 0.5 < M_* < 1.0 \\ 2.3 & \text{if} \quad 1.0 < M_* < 125 \end{cases} \tag{3.6}$$

where $M_* = M/M_\odot$. We assume the IMF to be both universal and constant in time. We compile the mass ranges we use in our calculations together with the number of stars per solar mass and fraction of mass locked up in the mass range estimated by the IMF in Table 3.4. The number of stars per solar mass displayed in the table is multiplied by the mass of newborn stars estimated from our semi-analytic models to yield the number of stars per redshift bin that we consider potential terrestrial planet hosts.

This choice of IMF is not fully consistent with L01 where it was assumed that 5% of the stellar mass was converted into solar-type stars in the mass range $M = 0.8 - 1.2M_\odot$. Instead, we get that $\approx$ 6.4% of the mass is converted into stars of said mass range. Although this difference may seem small in terms of percentile units, one must keep in mind that increasing the fraction of stellar mass converted to stars from 0.05 to 0.064 increases the total number of stars formed by 28%. Nevertheless, for the results tabulated in Table 4.1 we apply our choice of IMF to the calculations with the planet occurrence recipes from L01 and P08.

Table 3.4: Stellar mass ranges used in our calculations. $N_{\rm stars}$ is the number of stars per $M_\odot$ calculated from Equation 3.5 and $M_{\rm frac}$ is the fraction in percent of total mass locked up in the mass range.

Mass range ($M_\odot$)	0.08-0.60	0.60-0.80	0.80-1.00	1.00-1.20	0.13-1.34
$N_{\rm stars}$ (per $M_\odot$)	2.135	0.082	0.041	0.025	2.295
$M_{\rm frac}$(%)	42.12	5.67	3.67	2.70	55.71

3.3.2 Metallicity Distribution

In order to associate a metallicity to the stars forming at each redshift step of Δz we construct a metallicity distribution function. Similar to how we estimate the SFR from our models, we look at how much stellar mass has formed during small time intervals and what metallicity the star particles has. Each star particle is assigned to a metallicity bin in the range from $-3.0 <$ [Fe/H] $< +1$ with steps of 0.1 dex. We then calculate how much stellar mass is confined within each bin and normalise it to the total mass of stars formed in that time interval, thus constructing a probability distribution of metallicities at specific redshifts. This is done for $\geqslant 50$ redshifts with time intervals of ~ 260 Myr. This probability distribution is then interpolated to fit the redshift resolution of $\Delta z = 0.05$ in concordance with our SFR calculations. The mass that formed at each redshift step would then have a fraction of mass corresponding to the metallicity probability distribution. We also plot the mass-weighted mean metallicity in Figure 3.24.

Our planet occurrence recipe does not allow for terrestrial planets to form at metallicities [Fe/H] < -2.2, leaving lower metallicities unnecessary for our estimations albeit useful for plotting purposes.

3.3.3 Isochrones

Stars do not live forever and will eventually exhaust their hydrogen fuel, leave the main sequence and reach their final evolutionary stage. How long a star will fare on the main sequence is determined by parameters such as mass and metallicity. We have already determined these two factors in previous sections for our calculations, which we can use in order to figure out how many of the host stars in our estimations will have perished. From the stellar evolution models by Bressan et al. (2012) we acquire the appropriate *isochrones*[7] to aid our calculations. These isochrones tell us how long stars of a certain mass and metallicity will stay on the main sequence, which we include in our calculations.

[7] http://stev.oapd.inaf.it/cgi-bin/cmd

Combining our IMF calculations together with the metallicity distributions and the SFR, we acquired insight on the number of stars with certain metallicities and their age. Comparing then to the isochrones, we removed the number of stars that did not meet the criteria for a prolonged life on the main sequence. As we are only working with rather low-mass stars here, we do not concern ourselves with stars going supernovae upon completing their life-cycles. However, we assume that planets harboured by stars that evolve off the main sequence are destroyed along with their host star.

There are more things in heaven and earth, Horatio,
Than are dreamt of in your philosophy.
- **Hamlet (1.5.167-8)**, Hamlet to Horatio

4

Results

Here we present the results from our calculations. We investigate the differences in our models and recipes by altering various parameters, thus creating several more scenarios for possible outcomes. Our planet occurrence recipe is compared to those of L01 and P08 in Section 4.1.1, with their results for our two semi-analytic models shown in Table 4.1. We further compare the results from the models in Section 4.1.2, as well as the different results we get if we swap the SFR from the models with the theoretical cosmic SFH from Equation 3.3. We probe different combinations of power laws in Section 4.1.3 and in Section 4.1.4 we investigate the effects of our assumptions to the planet occurrence recipe, such as the gradual cutoff at the lower metallicity end. In Section 4.1.5 we make estimates of the number of terrestrial planets when our planet occurrence recipe is applied to more constrained stellar host parameters. We dub this the *observational regime*, which includes the mass- and metallicity range for host stars to which we have confirmed detections of terrestrial planets to date.

We further use our methods to estimate the number of main sequence stars in the observable Universe in Section 4.2 and compare the results with other estimates found in the literature. As an illustrative measurements, we also investigate our methods applied to the Large Magellanic Cloud and galaxies of similar mass to the Milky Way in Sections 4.3 & 4.4. Lastly, in Section 4.5 we apply our methods to estimate the number of terrestrial planets in the habitable zone of their host star and give a brief discussion about the prospects of habitability.

4.1 Number of Terrestrial Planets

Through our methods we estimate the number of terrestrial planets in our past light cone, conversely, the number of terrestrial planets in the observable Universe. We define the number of terrestrial planets as N_p and their typical age as $\bar{t}_{\rm age}$.

To briefly summarise our results: Within the observational regime of host star metallicity and mass where we have detected and confirmed the presence of terrestrial planets, we estimate a total number of terrestrial planets in the observable Universe to be $\log_{10}(N_p) \approx 20.425^{+0.439}_{-0.025}$. The typical age of those planets is estimated to be $\bar{t}_{\rm age} \approx 7.81^{+1.21}_{-0.28}$ Gyr. By lifting the conservative restrictions of the observational regime and include stellar hosts of a wider range of metallicities, we estimate the number of terrestrial planets in the observable Universe to be $\log_{10}(N_p) \geqslant 20.820^{+0.468}_{-0.001}$ and their typical age to be $\bar{t}_{\rm age} \approx 7.94^{+1.13}_{-0.20}$ Gyr. The errors are estimated to be our lower and upper limits based on the variation of star formation rates, metallicity distributions from the semi-analytic models and intrinsic errors in the power laws for the occurrence rate of giant planets.

4.1.1 Planet Occurrence Recipes

Because the work of L01 and P08 did not include M-dwarfs or observational occurrence rates for their planet recipes, we focus the comparison of the recipes to FGK-stars in particular. For the Durham model our planet occurrence recipe yields $\log_{10}(N_p) = 18.850$, which is almost 50% more than the estimated number with the L01 recipe ($\log_{10}(N_p) = 18.679$) but 4% lower than the estimated number with the P08 recipe ($\log_{10}(N_p) = 18.868$).

In comparison to the Durham model, Galacticus systematically predicts an increase in the number of planets for all planet recipes. The main reason for this discrepancy comes from the difference in total stellar mass predicted by the Galacticus model which has a much higher SFR at older times, something that is also reflected on the estimated typical age of the planets. However, our planet occurrence recipe estimates the number of terrestrial planets with the Galacticus model to be $\log_{10}(N_p) = 19.021$, which is lower than if we apply the planet formula of either L01 ($\log_{10}(N_p) = 19.049$) or P08 ($\log_{10}(N_p) = 19.176$). Despite having a much more generous range of metallicities for potential terrestrial planet hosts, our recipe predicts a lesser number of terrestrial planets. The reason behind this comes from the metallicity distribution predicted by the

Galacticus model, which will produce enough giant planets to reduce the number of terrestrial planets orbiting FGK-stars by a significant amount in our case. This effect is illustrated in Figure 4.1 where we plotted the time evolution of the planet occurrence recipes for different metallicity distributions.

Table 4.1: Results from our semi-analytical models for different planet-recipes prescribed in Section 3.1. All results are made with our assumption of the IMF so that $\approx 6.4\%$ of the total stellar mass is converted into FGK-stars in the mass range $0.8 - 1.2 M_\odot$.

Model: Recipe	Spectral type	Durham $\log_{10}(N_p)$	Durham $\bar{t}_{\rm age}$ (Gyr)	Galacticus $\log_{10} N_p$	Galacticus $\bar{t}_{\rm age}$ (Gyr)
Lineweaver	FGK	18.679	7.29	19.049	8.83
Prantzos	FGK	18.868	7.54	19.176	8.90
This work	FGK	18.850	7.75	19.021	8.96
This work	FGKM	20.921	7.74	21.288	9.07

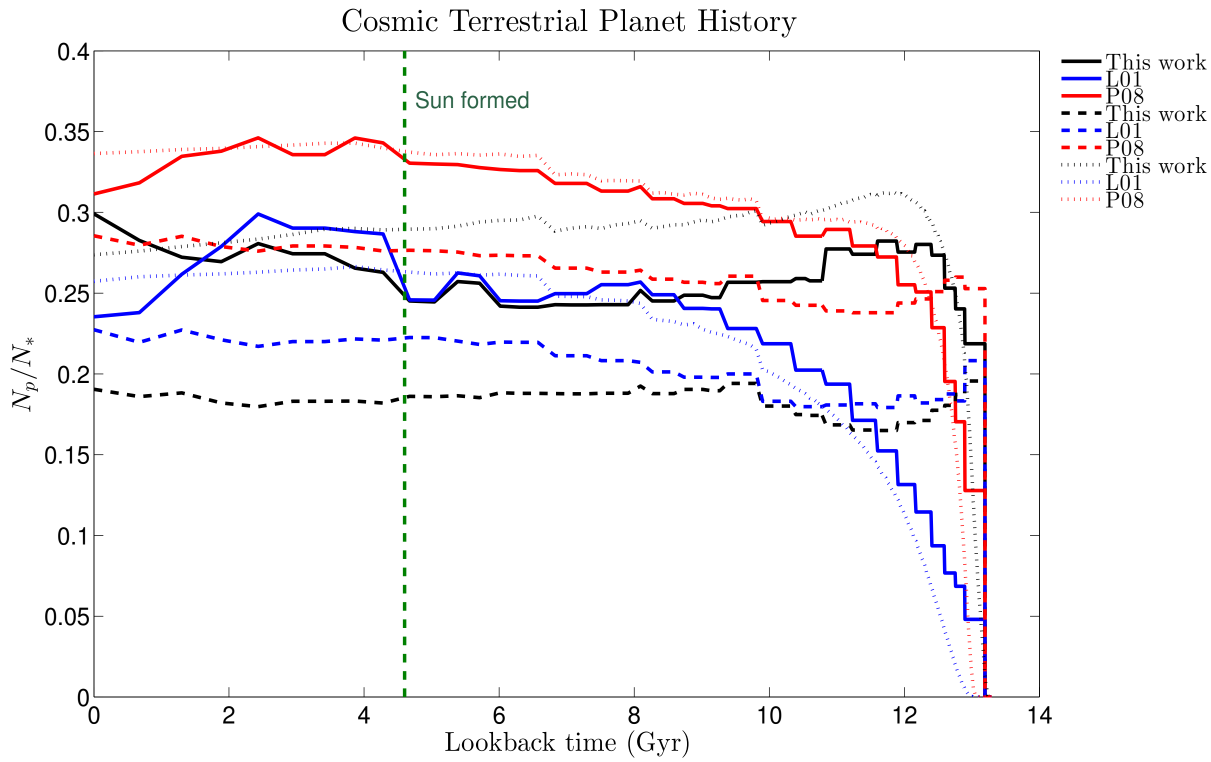

Figure 4.1: Probability for FGK-stars to harbour terrestrial planets over cosmic time. The black lines show the evolution of our planet occurrence recipe derived in this work, the blue line the work of Lineweaver (2001) and the red line that of Prantzos (2008). The solid lines show the cosmic evolution when adopting the metallicity distribution of the Durham model, the dashed lines the metallicity distribution predicted by Galacticus and the dotted lines the metallicity evolution of Equation 3.4. The green dashed line acts as an indicator for when the Sun was formed. Note that the planet occurrence recipes from Lineweaver (2001) & Prantzos (2008) have been used here with our SFR and metallicity distributions and not in accordance to their original estimates.

4.1.2 Model Comparison

Leaving the L01 and P08 planet occurrence recipes behind and fixating on the one presented in this work, we narrow down the research to our different models instead. In Figure 4.2 we show the estimated number of terrestrial planets for each model at different redshifts in bins of size $\Delta z = 0.05$. We can see from the figure that the Galacticus model predicts more planets for most of the time at redshifts $z \leqslant 9$, with a peak in number of planets for both models at $z \sim 2$. This substantial production of planets at earlier times for the Galacticus model is then translated into an older typical age. A plot of the typical age of planets at redshifts $z \leqslant 3$ is shown in Figure 4.3. Because not much time has elapsed between higher redshifts, the typical age of terrestrial planets is similar above redshift $z \geqslant 3$. We also compare the fraction of terrestrial planets above a certain age threshold, shown in Figures 4.4 & 4.5 for redshifts $z = 0.0, 0.2, 0.5, 1.0$ & 2. Note the broader shape of the Galacticus model, indicating a higher terrestrial planet population above the different age thresholds.

In order to account for plausible deficiencies with the SFH from our semi-analytic models, we explore the outcome of combining the literature SFR of Equation 3.3 from Madau & Dickinson (2014) with the metallicity distributions our models predicted.

The resulting number of terrestrial planets in the observable Universe is $\log_{10}(N_p) = 20.820$ for the metallicity distribution of the Durham model and $\log_{10}(N_p) = 20.825$ for the Galacticus model. These results are both lower than the results of the SFH from the respective model, due to the overall reduced SFR predicted by the literature (c.f. $\log_{10}(N_p) = 20.921$ for Durham and $\log_{10}(N_p) = 21.288$ for Galacticus). The typical age of planets is also very similar when comparing the two metallicity distributions, being $\bar{t}_{\rm age} = 7.98$ and 8.00 Gyr for the metallicitiy distributions of the Durham and Galacticus model respectively (c.f. $\bar{t}_{\rm age} = 7.74$ and 9.07 Gyr from the corresponding SFR of each model). We further probe the effect of the two different metallicity distributions applied to the literature same SFH for some special scenarios in Section 4.1.4.

4.1.3 Power Law Variation

By probing different combinations of planet recipes (i.e. occurrence rate power laws for giant planets), metallicity distributions and SFR we get quite varied results. The parameters for the power law ($f_{\rm Giants} = f_0 10^{a[\rm Fe/H]} M_*^b$) describing the occurrence of giant planets in our planet recipe was obtained from GM14 as $f_0 = 0.07, b = 1$ with

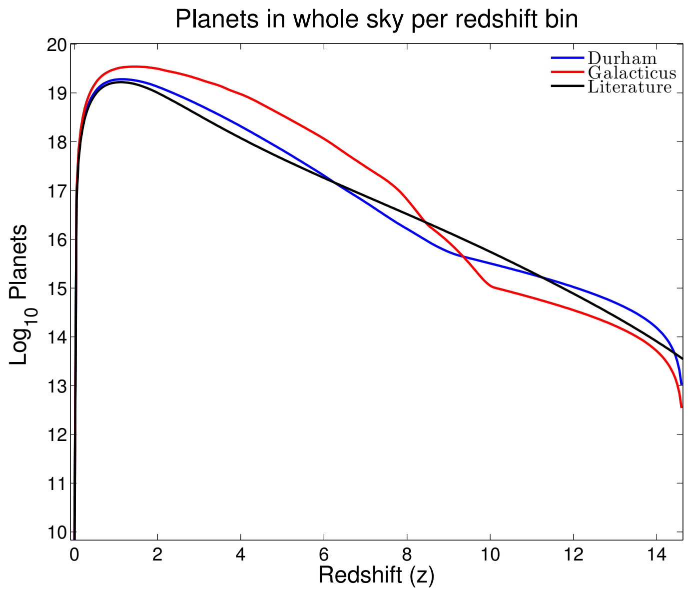

Figure 4.2: Logarithm of the estimated number of terrestrial planets in the sky in different redshift bins of size $\Delta z = 0.05$ from our planet occurrence recipe and semi-analytic models. The models predicts about the same amount of planets at redshift $z \approx 9$, about ~ 250 million years after terrestrial planets started to form at redshift $z = 14.6$. We also include an estimate of the number of planets predicted by the theoretical values from Equation 3.3 and 3.4, depicted by the black line in the figure. The number of planets drops steeply at redshift $z \approx 0$ because the comoving volume at lower redshift is so small.

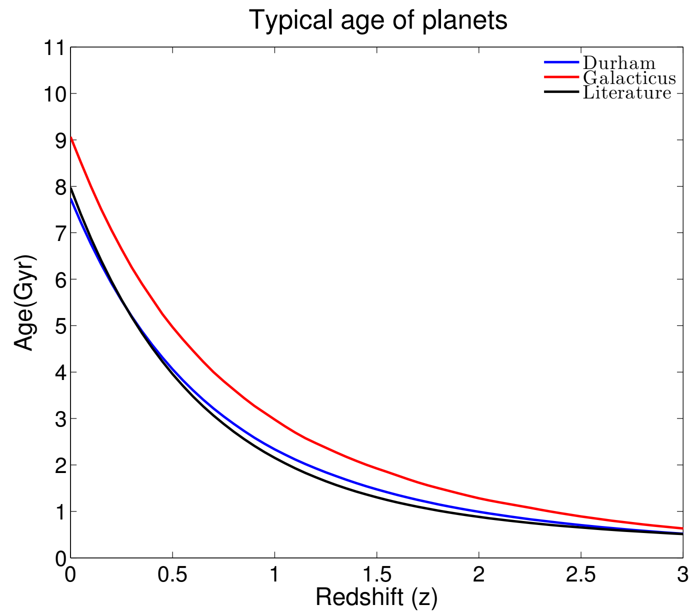

Figure 4.3: The typical age of terrestrial planets at specific redshifts predicted by our planet occurrence recipe and semi-analytic models. We also include an estimate of the number of planets predicted by the theoretical values from Equation 3.3 and 3.4, depicted by the black line in the figure.

$a = 1.06 \pm 0.42$ for M-dwarfs and $a = 1.80 \pm 0.31$ for FGK-stars. We listed a few other power law indices in Table 3.3 which we also tested together with our semi-analytic models. For the Durham model we modestly change our result by a reduction of $\sim 10\%$ in total amount of terrestrial planets in the observable Universe when we apply the power law index of Neves et al. (2013) for our M-dwarfs. For the Galacticus model the difference is greater however, with a reduction of $\sim 30\%$ in total amount of terrestrial planets. The power laws described by GM14 and Johnson et al. (2010) yield the same results for each semi-analytic model within three decimals marginal. The estimated typical age of terrestrial planets does not change by more than a few million years for the different combinations except for the Neves et al. (2013) power law with the Durham model, where the average age is increased to 7.85 Gyr from 7.74 Gyr.

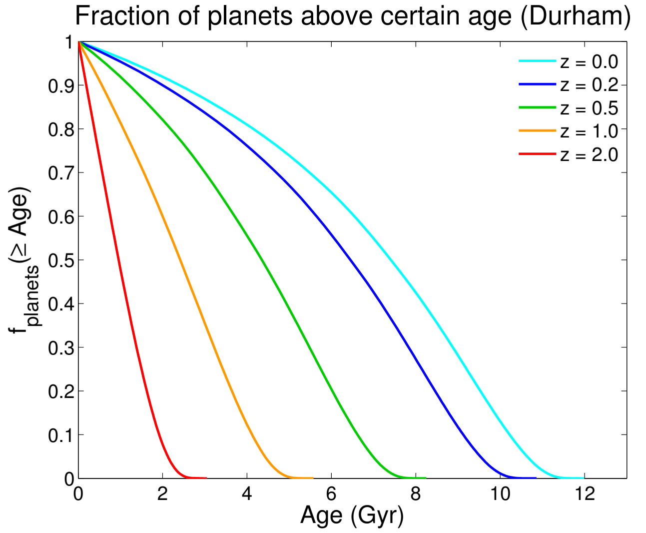

Figure 4.4: Fraction of planets at different redshifts above a certain age predicted by our planet occurrence recipe and the Durham semi-analytic model.

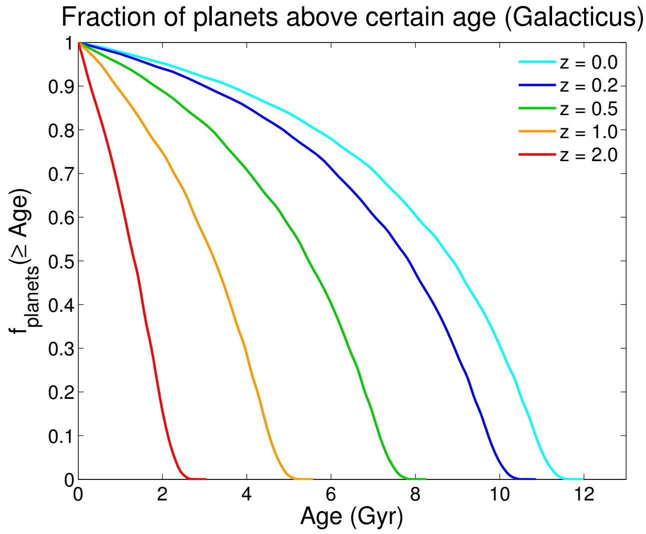

Figure 4.5: Fraction of planets at different redshifts above a certain age predicted by our planet occurrence recipe and the Galacticus semi-analytic model.

The power law fitted to our planet occurrence recipe carried an uncertainty of $\sigma_{a,\mathrm{M}} = \pm 0.42$ for M-dwarfs and $\sigma_{a,\mathrm{FGK}} = \pm 0.31$ for FGK-stars. Introducing these errors as upper and lower limits to the occurrence rate of giant planets altered the estimated number of terrestrial planets by a maximum of $\leqslant 10\%$ for FGK-stars and $\leqslant 2\%$ for M-dwarf. These errors are not presented in the tables to avoid cluttering.

4.1.4 Metallicity Relevance

Because some parts of our planet recipe is based on guesswork, e.g. the gradual cut-off at the lower metallicity end, we want to examine the robustness of this conjecture. We experiment with some different scenarios and compile noteworthy combinations and their results in Table 4.2. These cases also involve iterations with the metallicity distributions from our semi-analytic models applied to the theoretical SFH calculated with

Equation 3.3.

By assuming a flat occurrence rate at the lower metallicity end to [Fe/H]$= -2.2$, we see how our gradual cutoff effects the estimated number of terrestrial planets. For both semi-analytic models the change is small, with an increase just above $\sim 3\%$ for the Durham model and $\approx 0.5\%$ for the Galacticus model. We also probe the event of a flat occurrence rate at low metallicity with a steep drop in occurrence rate to zero at [Fe/H]$= -1.2$. In this case the Durham- and Galacticus models lost $\sim 6\%$ and 0.5% of the planets they had with a gradual cutoff towards lower metallicities respectively, suggesting that most terrestrial planets are formed at higher metallicities. We also probe the event of an absent need for heavy elements in order to form terrestrial planets and let the occurrence rate be flat at lower metallicities, extending all the way to zero. This case is not very different from the case with a flat occurrence to [Fe/H]$= -2.2$, yielding very similar results. The difference between the two cases is the largest for the Durham model, with $\log_{10}(N_p) = 18.6$ more terrestrial planets formed in the no cutoff scenario. As it is very unlikely that terrestrial planets would be able to form at this extremely low metallicity regime, the result vouches for this many stars to be unable to form terrestrial planets.

In order to further investigate the importance of the metallicity distributions for the estimated number of terrestrial planets in the observable Universe, we run our calculations without including the prevalence of giant planets. In other words, we include a case for which the probability to form terrestrial planets gradually increased from $-2.2 <$[Fe/H]< -1.2 to its maximum occurrence and that they do not get destroyed by giant planets. The results of this case is displayed in Table 4.2 under the note "No giant planets". The difference from our standard case was again modest, only an increase in number of terrestrial planets by $1 - 3\%$ and $\lesssim 10$ million years difference in mean age for both models. This case also scrutinises the relevance of our theory that giant planets destroy terrestrial planets in their vicinity.

We also probe the effect of applying the different metallicity distributions obtained from the semi-analytic models to the SFH of the literature for these cases. We note that the results are quite robust, only yielding a modest difference of $\lesssim 5\%$ in number of planets between the two metallicity distributions for the cases tabulated in Table 4.2.

Table 4.2: Results for special scenarios from our calculations using different combinations of star formation rates and metallicity distributions from our semi-analytic models and theoretical estimates from the literature with Equation 3.3. All results in the table are for FGKM-stars in the range $M = 0.08 - 1.2M_\odot$ except for the special cases noted as "Observational regime" where we only assume host stars with $M = 0.13 - 1.34M_\odot$ and $-0.55 <$ Fe/H $< +0.33$ to be able to harbour terrestrial planets.

SFR	$Z-$distribution	$\log_{10}(N_p)$	$\bar{t}_{\mathrm{age}}$ (Gyr)	Notes
Durham	Durham	20.937	7.77	No cutoff
Galacticus	Galacticus	21.290	9.07	No cutoff
Literature	Durham	20.831	8.00	No cutoff
Literature	Galacticus	20.823	8.00	No cutoff
Durham	Durham	20.935	7.77	Cutoff at [Fe/H]< -2.2
Galacticus	Galacticus	21.290	9.07	Cutoff at [Fe/H]< -2.2
Literature	Durham	20.830	8.00	Cutoff at [Fe/H]< -2.2
Literature	Galacticus	20.823	8.00	Cutoff at [Fe/H]< -2.2
Durham	Durham	20.892	7.69	Cutoff at [Fe/H]< -1.2
Galacticus	Galacticus	21.283	9.06	Cutoff at [Fe/H]< -1.2
Literature	Durham	20.792	7.93	Cutoff at [Fe/H]< -1.2
Literature	Galacticus	20.816	7.99	Cutoff at [Fe/H]< -1.2
Durham	Durham	20.927	7.73	No giant planets
Galacticus	Galacticus	21.303	9.06	No giant planets
Literature	Durham	20.823	7.97	No giant planets
Literature	Galacticus	20.835	7.99	No giant planets
Durham	Durham	20.513	7.53	Observational regime
Galacticus	Galacticus	20.864	9.02	Observational regime
Literature	Durham	20.425	7.81	Observational regime
Literature	Galacticus	20.400	7.96	Observational regime

4.1.5 Observational Regime

In order to further test the restrictions of our planet occurrence recipe, we include a case where we only allow an occurrence rate for planets within the confined metallicity range we have observations of confirmed terrestrial planets. This case is noted as "Observational regime" in Table 4.2 and displayed by the shaded area in Figure 3.8. We restrict this observational regime to metallicities between $-0.55 \lesssim$[Fe/H] $\lesssim +0.33$, according to most metal-poor terrestrial planet host star (Kepler-444, Campante et al. 2015) and the most metal-rich terrestrial planet host star (Kepler-407, Marcy et al. 2014) observed so far. In addition to a metallicity limit we also include restraints on the mass of the host star to be within the interval $M = 0.13 - 1.34M_\odot$. This mass constraint is based on the least massive and most massive star observed to harbour terrestrial planets and not correlated to the metallicity constraint we imposed (Kepler-42 and Kepler-21 respectively, Borucki et al. 2011).

Compared to the calculation of our original planet occurrence recipe and its restrictions, the observational regime shows a decreased number of terrestrial planets by $\approx 60\%$ for both metallicity distributions predicted by our models. In other words, our planet occurrence recipe predicts ≈ 2.5 times more terrestrial planets than what is observed in the planet host samples we have today. Our planet occurrence recipe also predicts an older terrestrial planet population. In the observational regime we estimate the typical age of planets to be $\bar{t}_{\rm age} = 7.53$ Gyr for the Durham model and $\bar{t}_{\rm age} = 9.02$ Gyr for the Galacticus model. With the full appliance of our planet occurrence recipe, we get an increase of the typical age by ≈ 210 Myr and ≈ 50 Myr for the Durham and Galacticus model respectively.

When we examine the different metallicity distributions from the semi-analytic models applied to the literature value of the cosmic SFH, we get the number of terrestrial planets to $\log_{10}(N_p) = 20.425$ & 20.400 for the Durham and Galacticus model metallicity distributions respectively. Although the Galacticus metallicity distribution predicts fewer terrestrial planets, the typical age is ≈ 150 Myr higher than what the Durham model predicts (c.f. $\bar{t}_{\rm age} = 7.81$ Gyr for the Durham metallicity distribution and $\bar{t}_{\rm age} = 7.96$ Gyr for Galacticus). The difference in typical age is generally smaller for the other cases with the same SFH tabulated in Table 4.2. This discrepancy is due to the chemical evolution predicted by the different models and the strict constraints on metallicity in the observational regime. For the Durham model metallicity gradually builds up over time and estimates more terrestrial planets at lower redshifts. The metallicity distribution from Galacticus model on the other hand predicts planets to form even at high redshifts, albeit fewer as the metallicity is sufficient enough to produce giant planets instead.

4.2 Number of Stars in the Observable Universe

In Table 4.3 we give the estimated number of stars in the observable Universe, N_*, for our three different cosmic SFH as well as their average age. We also compare the estimated average age of stars with some of the literature found. We need to point out that the mean age of stars we estimate with the literature SFH of the best fit function derived by Madau & Dickinson (2014) as $\bar{t}_{\rm age} \approx 8.00$, differs slightly from the value they prescribe in their review of $\bar{t}_{\rm age} \approx 8.30$ Gyr. As we use the same cosmology as Madau & Dickinson (2014), we believe this discrepancy is caused by the different treatment of long-lived stars with isochrones and numerical differences such as resolution in timesteps.

Table 4.3: Number of stars in the observable Universe and their typical age. The values estimated in this work are lower limits with uncertainties from using different cosmologies.

SFR	N_*	$\bar{t}_{\mathrm{age}}$ (Gyr)
Durham	$9.57^{+0.45} \times 10^{20}$	$7.77^{+0.19}$
Galacticus	$2.20^{+0.21} \times 10^{21}$	$9.07^{+0.23}$
Literature	$7.59^{+0.75} \times 10^{20}$	$8.00\ ^{+0.21}$
Madau & Dickinson	-	8.30
Gallazzi et al.	-	9.00

We can also compare our estimated number of stars in the observable Universe to other estimates found on the web. NASA estimated the number of stars to be on the order of $\sim 10^{21}$ in 2005 by looking at the Hubble Deep Space Image of the Virgo Cluster and assuming that the sky was uniform with approximately the same amount of stars and galaxies over all directions. This number ranges a lot depending on what assumptions one makes. On the European Space Agency (ESA) webpage one finds the approximate number of stars in the observable Universe to be between $10^{22} - 10^{24}$ by assuming all visible galaxies to be similar to the Milky Way in number of stars [1]. The NASA FERMI mission measured gamma rays in order to estimate all the stars that has ever shone in the observable Universe, yielding $\approx 5.9 \times 10^{21}$ stars (estimated from an average density of 1.4 stars per 100 billion cubic lightyear)[2].

4.3 Large Magellanic Cloud

As a simple exercise, we can apply our planet recipe to the *Large Magellanic Cloud* (LMC) and estimate how many stars of our neighbouring galaxy harbour terrestrial planets. Studies by Kim et al. (1998) of the LMC have suggested a disk stellar mass of $M_{\mathrm{LMC}} \approx 2 \times 10^9 M_\odot$ which is thought to not have undergone any starburst epochs in its lifetime. A stellar age and metallicity distribution of field stars found in the LMC by Piatti & Geisler (2013) is presented in Table 4.4. From this data we can simply apply the stellar mass of the Large Magellanic Cloud to our initial mass function to estimate the number of stars that could potentially harbour terrestrial planets that avoid being destroyed by voracious giant planets. With this simple data at our disposal we obtain the of the number of terrestrial planets in the LMC to be of order $\log_{10}(N_p) \approx 9.634$ with a typical age of $\bar{t}_{\mathrm{age}} \gtrsim 5.51$ Gyr.

[1] http://www.esa.int/Our_Activities/Space_Science/Herschel/How_many_stars_are_there_in_the_Universe

[2] http://www.spaceflightnow.com/news/n1211/01fermi/#.VUZKCXWsU8o

Table 4.4: Age and metallicity of field stars in the Large Magellanic Cloud obtained from Piatti & Geisler (2013).

Age (Gyr)	Metallicity Fe/H
1.2	-0.32
2.0	-0.50
2.6	-0.55
3.2	-0.59
4.0	-0.69
5.0	-0.71
6.4	-0.80
8.1	-0.87
10.1	-0.91
12.7	-0.89

Perhaps the most interesting result from this estimation is that even though the LMC has quite metal-poor stellar population, we estimate that most terrestrial planets are almost 1 Gyr older than Earth. Another reason which makes our result alluring is that the LMC, being a close neighbour to the Milky Way, will be a good candidate to make future extragalactic exoplanet observations in to test our results. Such observations may already be possible with e.g. microlensing techniques (Dominik 2012; Jetzer 2008).

4.4 The Milky Way

From our semi-analytic models we obtain a number of galaxies of similar mass as the Milky Way which we can use to assess a rough estimate of the number of terrestrial planets in our galaxy. By extracting the galaxies from the models within the mass range $4.6 - 6.43 \times 10^{10} M_\odot$, we have a sample of galaxies within the estimated stellar mass range of the Milky Way (Licquia & Newman 2013; McMillan 2011). As we already know both the chemical evolution and the SFH of these galaxies from our models, we can apply our planet occurrence recipe and estimate the number of terrestrial planets and the typical age of said planets for each galaxy. Our estimates suggest that the number of terrestrial planets in a galaxy of similar mass as the Milky Way should be $\log_{10}(N_p) \approx 10.958 - 11.122$. Both our models predict very similar amount of terrestrial planets for galaxies in this mass range, with the lower and upper limit suggested here coming from the stellar mass constraints of the Milky Way. However, the mass-weighted mean age ranges from 7.77 Gyr to 8.44 Gyr for the Durham and Galacticus model respectively. This discrepancy between the models is due to the very old population of stellar particles the Galacticus model predicts, depicted by the red line in Figure 4.6

where we plot the age distribution of terrestrial planets in galaxies of this mass range.

If we compare this result to the literature, we find that our estimates predict an older population of terrestrial planets compared to e.g.Lineweaver et al. (2004), where the average Earth-like planet in the Galaxy is estimated to be ≈ 5.5 Gyr. Guo et al. (2009) estimates the number of terrestrial planets in the Milky way to be $\log_{10}(N_p) \approx 10.658$, whereas we estimate the number to be at least twice as much. However, Guo et al. (2009) estimates the number of terrestrial planets in the habitable zone which could explain the disparity. Our estimate of the average age of $\bar{t}_{\rm age} \sim 7.77 - 8.44$ Gyr is also older than the average age of Earth-like planets orbiting FGK-stars that L01 appraises to be 6.4 ± 0.9 Gyr. The star formation history and chemical evolution of the Galaxy may not be very well represented by our models, which does not necessarily account for the same epochs of starbursts as the Milky Way have undergone (Rocha-Pinto et al. 2000).

Figure 4.6: Estimated terrestrial planet fraction residing in galaxies with similar mass as the Milky Way predicted by our semi-analytic models. Note that it is the age of the planets that is plotted in log scale on the x-axis and not the galaxies.

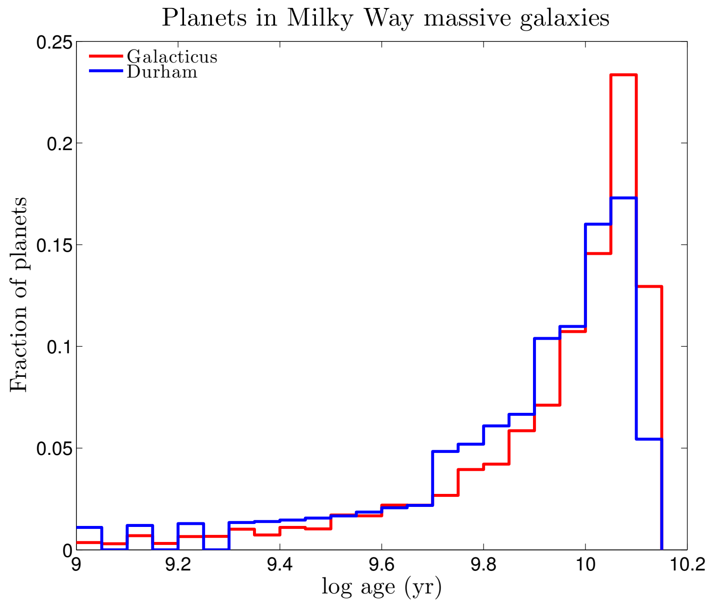

4.5 Habitability

Much of the work in exoplanetary astronomy of late has been towards finding exoplanets within the *habitable zone* (e.g. Farr et al. 2014; Guo et al. 2009; Kopparapu 2013). Indeed, this was one of the main purposes of the *Kepler* mission[3] and these days we are able to make some statistics on the presence of exoplanets in the habitable zone of low-mass stars (e.g. Bonfils et al. 2013; Tuomi et al. 2014; DC15). Definitions of

[3] http://exep.jpl.nasa.gov/documents/ExoplanetCommunityReport.pdf

the habitable zone may vary some in the literature, but the most accepted definition is the *moist greenhouse* habitable zone of Kasting et al. (1993). This definition of the habitable zone describes the distance from the host star to which a planet may have sustained liquid water on its surface. The simplest depiction would be that a distance too far from the star would cause the water to freeze whereas a distance too close would cause the water to evaporate from the surface of the planet. Because stars of various masses exposes the planet to different amount of flux, the habitable zone is dependent on the spectral type of the star as well as the size of the planet. Stars of low mass such as M-dwarfs have their habitable zone quite close to the host star, making detections of planets in the habitable zone of such stars a possibility (e.g. Quintana et al. 2014). However, due to the limitations of our current technology, observing terrestrial planets in the habitable zone of Sun-like stars has proven to be quite a predicament. Both Doppler and transit method techniques suffer greatly when trying to detect terrestrial planets on wider orbits around Sun-like stars as those planets do not interact with the host star above current noise levels. Nevertheless, to go about this issue one usually applies modest extrapolation of shorter orbits unto longer ones (e.g. Petigura et al. 2013).

Recently, Kopparapu et al. (2013) revised the constraints of the moist greenhouse habitable zone to include terrestrial planets of a wider range of sizes and host stars with lower surface temperatures than those derived by Kasting et al. (1993). Other definitions involve the total amount of flux hitting the planet to be within a certain range, e.g. $F_P = 0.25 - 4.00F_\oplus$ (Petigura et al. 2013). Generous definitions may include the distances of an early Mars and Venus as outer and inner limits for the habitable zone (e.g. Selsis et al. 2007). Cloud formation due to planetary rotation was investigated by Yang et al. (2014a), suggesting that stable atmospheres may be more common than earlier believed. Recent *Kepler* data of the occurrence rate of planets orbiting M-dwarfs in a vivid selection of definitions of habitable zones is tabulated by DC15.

An analogous interpretation to express terrestrial planets in the habitable zone is the common usage of the name "η-Earth". Just as with the habitable zones themselves, $\eta-$Earth may have various definitions in the literature, albeit the meaning is in principle the same. Here we employ our calculations to estimate the number of terrestrial planets in the habitable zone, or how many $\eta-$Earths we expect there are in the observable Universe. Extrapolation of planet occurrences found by *Kepler* has yielded a fraction of $f_\eta \approx 0.1$ planets with size $R = 1 - 2R_\oplus$ per Sun-like star in the habitable zone (Batalha 2014; Petigura et al. 2013). Kopparapu (2013) revised the occurrence rate of rocky planets ($R = 0.5 - 1.4R_\oplus$) in the habitable zone estimated by DC13 to include planets of size $R = 0.5 - 2.0R_\oplus$ to be $f_\eta \approx 0.5$. By applying these occurrence rates for terrestrial planets in the habitable zone to our calculations, we wind up with the results shown in Table 4.5.

Our results of the estimated number of $\eta-$Earths is based on current occurrence rate estimates of terrestrial planets the habitable zone of Kopparapu et al. (2013). This definition involves a habitable zone of which the planet receives roughly the stellar flux of $F_P \approx 0.35 - 1.01 F_\oplus$, also known as the maximum greenhouse- and moist greenhouse limit. We could easily apply a different definition and other occurrence rate, however that would only scale our results accordingly to the difference in planet occurrence rates. From our calculations we obtain the number of $\eta-$Earths in the observable Universe to be $\log_{10}(N_\eta) \geqslant 20.509^{+0.464}_{-0.003}$, with a typical age of $\bar{t}_{\mathrm{age}} \approx 7.98^{+1.09}_{-0.23}$ Gyr. The uncertainties of our estimates originate from the results of our different SFH, metallicity distributions and giant planet occurrence power law. If we restrict ourselves to the observational regime of which terrestrial planets have been observed, the estimated number of $\eta-$Earths in the observable Universe is reduced to $\log_{10}(N_\eta) \geqslant 20.107^{+0.291}_{-0.021}$, with the typical age of $\bar{t}_{\mathrm{age}} \approx 7.82^{+1.20}_{-0.28}$ Gyr.

4.5.1 Discussion on Habitability

A question that remains open at the moment is whether M-dwarfs can be associated with habitability in the same sense as Sun-like stars (Scalo et al. 2007). Extreme Ultraviolet (EUV), X-ray radiation and flares exhibited by low-mass stars may drastically erode a stable atmosphere and therefore the prospects of habitability (e.g. Luger & Barnes 2015; Scalo et al. 2007; Segura et al. 2005). Sengupta (2015) investigated the ratio between

Table 4.5: Results for our estimation of the number of $\eta-$Earths in the observable Universe as well as the mean age. Here we applied the same planet recipe discussed in Section 3.1 but reduce the occurrence rate of terrestrial planets to fit that of the observed in the habitable zone. The note "Observational regime" indicates where we only counted host stars with $M = 0.13 - 1.34 M_\odot$ and $-0.55 < \mathrm{Fe/H} < +0.33$ to be able to harbour terrestrial planets.

SFR	$Z-$dist	$\log_{10} N_p$	$\bar{t}_{\mathrm{age}}$ (Gyr)	Notes
Durham	Durham	20.611	7.75	FGKM
Galacticus	Galacticus	20.973	9.07	FGKM
Literature	Durham	20.509	7.98	FGKM
Literature	Galacticus	20.511	8.00	FGKM
Durham	Durham	20.196	7.54	Observational regime
Galacticus	Galacticus	20.544	9.02	Observational regime
Literature	Durham	20.107	7.82	Observational regime
Literature	Galacticus	20.086	7.97	Observational regime

EUV and bolometric luminosities of low-mass stars hosting planets in the habitable zone. The survey estimated that only a handful of the M-dwarfs with confirmed planets in the habitable zone met the criteria for having Earth-like habitable conditions. Another issue with low-mass hosts is that due to the habitable zone being so close to the star, planets within it may experience *synchronous rotation* and be tidally locked (Kasting et al. 1993). Such planets would have a constant "day"-side towards the host star and an everlasting "night"-side facing the other way. Volatile compounds that make up the atmosphere and oceans of the planet may freeze out to form a giant ice cap on the dark side, causing an atmospheric collapse if it gets too cold (Segura et al. 2005). Whether tidally locked planets can attain hospitable environments or not remains disputable but some simulations and theories suggest that they may achieve Earth-like conditions under special circumstances (e.g. Angerhausen et al. 2014; Joshi et al. 1997; Yang et al. 2013, 2014b). Yang et al. (2013) argue that cloud formation may greatly increase the planetary albedo and reduce the surface temperatures, a phenomenon that may even reduce the contrast between day- and nightside of the planet. The presence of substellar water clouds and the proposed clement surface conditions of tidally locked planets is something that may be detectable with upcoming missions such as the James Web Space Telescope.

Another subject for debate is the prevalence of wet *water worlds*, dry *desert worlds* and the possibility for such planets to be habitable (e.g. Goldblatt 2015). Interior structure of the planet plays an important role in regulating the temperature of the planet via heat losses from the core and drives the long term volatile cycling between interior, atmosphere and oceans on the planet (Noack et al. 2014; Tackley et al. 2014). Plate tectonics can determine the outcome for land mass and depths of the oceans of the planet (Sleep 2005). As we can see, there are many parameters to consider than just the distance to the host star when it comes to habitability of the planet. There is also the matter of the longevity of a planet to be within the habitable zone, or the *continuous habitable zone* (CHZ) as it may be referred to (Rushby et al. 2013). As the host star evolves during its lifetime, so does the habitable zone as well. Rushby et al. (2013) compiled estimates of the CHZ for stars of different masses and compared them to the position of the Earth and the exoplanet Gliese 581d, seen here in Figure 4.7. The habitable zone may even evolve along with the star so that planets do not enter the habitable zone until after the star has evolved away from the main sequence (Guo et al. 2010). As low-mass stars do not evolve very quickly and stay on the main sequence for a long time, the CHZ is wider around them. Because M-dwarfs are much more common than other types of stars and have wide CHZs, they have become targets of high interest for astrobiologists in the pursuit of habitable worlds.

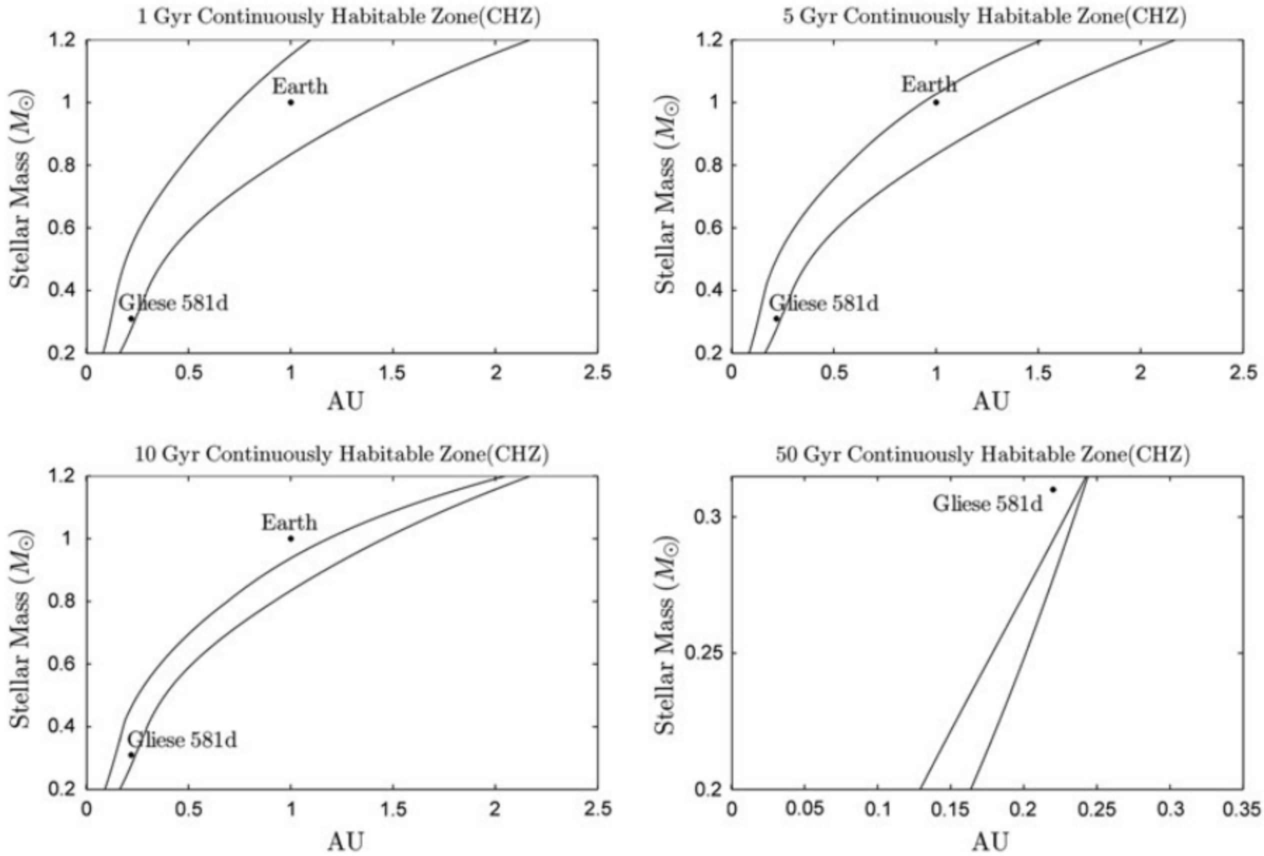

Figure 4.7: Continuous Habitable Zones for 1, 5, 10 and 50 Gyr for stars with mass ranging from $0.2 - 1.2M_\odot$. Earth and Gliese 581d are included for reference. Note the scale change of both axes for the 50 Gyr CHZ in the bottom right plot. Courtesy of Rushby et al. (2013).

It has also been suggested by e.g. Cockell (2014) that the habitable worlds may not at all have the requirements we demand of them. By examining more extreme, rarely encountered habitats on Earth which are more common on other planetary bodies, we may expand our description of habitability. We do not consider a *Galactical habitable zone* or dangerous events for habitability such as supernova-sterilisation for our calculations (Gonzalez 2005, 2014; Gonzalez et al. 2001; Lineweaver et al. 2004). In none of our calculations do we account for the possibility of exoplanetary moons to be habitable, which may very well contribute to the number of habitable worlds (e.g. Heller et al. 2014; Hinkel & Kane 2013). Neither do we cover the possibility of free-floating planets to be habitable (Badescu 2011).

5

I told her we were going to get married, and all she could talk about was frogs. She said there's these hills where it's hot and rains all the time, and in the rainforests there are these very tall trees and right in the top branches of the trees there are these like great big flowers called... bromeliads, I think, and water gets into the flowers and makes little pools and there's a type of frog that lays eggs in the pools and tadpoles hatch, and grow into new frogs and these little frogs live their whole lives in the flowers right at the top of the trees and don't even know about the ground, and once you know the world is full of things like that, your life is never the same.

— Masklin, Terry Prattchet's The Bromeliad Trilogy

Conclusions

PROGRESS in our understanding of the formation and evolution of planetary systems has been remarkably favourable in recent years. Exoplanetary astronomy is indeed in a flourishing state and with upcoming space missions such as PLATO and TESS, the prospects for further development are looking good. While much effort in exoplanetary research is going towards trying to find systems reminiscing of our own, we have learned that although the Solar system seems to be a rare specimen, terrestrial sized planets are quite abundant in the Galaxy. In this work we asses the number to be to be $\log_{10}(N_p) \sim 20.82 - 21.29$ in the observable Universe. In the following sections we discuss the meaning of the results we obtained, as well as some of assumptions we made in our estimates. We also give some insight to future prospects in Section 5.2.1.

5.1 Discussion

The planet occurrence rates adopted here are composed from the most recent results from transit and RV surveys. However, these methods are not without their limitations. The *Kepler* mission utilises the transit method in order to detect exoplanets which becomes increasingly difficult with increasing orbital radius of the planet. Doppler surveys also suffer from the same limitation in the way that low-mass planets on large orbits do not interact enough with the host star to cause signals above noise level. These issues limits the observed occurrence rates of terrestrial planets to shorter periods, which has to be corrected for incompleteness. In turn, estimates via extrapolation of planet occurrence rates to longer periods can sometimes be quite bold (e.g. Petigura et al. 2013).

Another way to go about this problem is to complement one method with another, for instance RV with microlensing studies (e.g. Clanton & Gaudi 2014; Montet et al. 2014). The advantage of microlensing is that such surveys may detect planets at much longer periods than what RV generally do for the same type of planets. However, combined surveys are not without their flaws either. Doppler surveys typically target stars in the Solar neighbourhood of a few pc away, whereas microlensing targets are usually at distances $d > 1$ kpc away in the direction of the Galactic bulge (Rolleston et al. 2000). The characteristics of targets from those different methods may not be the same or at all well determined (Gaudi et al. 2002). We discussed earlier in Section 3.1.3 that estimates of the occurrence rate of giant planets may change drastically for a small sample when the metallicity distribution of targeted stars and detected planets is altered.

Our method, especially the planet occurrence recipe, is very sensitive to the statistical estimates of the occurrence rates of planets. We assume a maximum occurrence rate of 0.4 terrestrial planets per FGK-star and 1 per M-dwarf. These occurrence rates are based on extrapolations of planets on shorter orbital periods and were corrected for incompleteness in the surveys they were obtained from. One may want to be more cautious when applying these occurrence rate estimates and limit the value to planets on shorter orbits where we have better statistics of confirmed exoplanets.

5.1.1 Planet Occurrence Recipe

One might argue that our planet occurrence recipe for harbouring terrestrial planets is quite generous. We have not observed any terrestrial planets (or any planets at all[1]) orbiting main sequence stars below [Fe/H]< -0.8, yet we assume a near-full occurrence rate even at this low metallicity. The reason behind the lack of detected planets at lower metallicities is not necessarily because there are no planets orbiting metal-poor stars, but rather because of the limitations in observations. RV surveys have a limited range and thus cannot observe potential planet hosts that are very far away and metal deficient. Faint, distant stars go undetected by e.g. *Kepler*, not to mention that it is quite difficult to accurately determine the metallicity of faint stellar populations (e.g. Mann et al. 2013). We introduced an "observational regime" to our planet occurrence

[1] http://exoplanets.org/, May 21, 2015

recipe to which we argued that the most metal-poor and metal-rich host stars observed serves as boundaries. These boundaries are very susceptible to change as our observational techniques improve and better constraints of target host stars can be acquired. In fact, the most ancient and metal-poor planetary system confirmed to date was observed by Campante et al. (2015) to be orbiting a host star of [Fe/H]= -0.55. Earlier measurements of the same star have yielded metallicities ranging down to [Fe/H]$\leqslant -0.70$ (Soubiran et al. 2008), suggesting that we may already want to revise our observational regime this very moment.

We probed our assumption of the gradual cutoff at the low-metallicity end of our planet occurrence recipe in Section 4 & Table 4.2. We noted that the results were not significantly altered by replacing the steadily decreasing probability to form terrestrial planets with a steep drop instead. The gradual cutoff itself was based on the heavy element abundance left in the minimum mass solar nebula in order to form a terrestrial planet, which we set as [Fe/H]$\geqslant -2.2$. This limit can be questioned as not necessarily all of the heavy elements end up in the planets. Nevertheless, we expect there to be a lower limit to the probability of which to be able to form a terrestrial planet based on the heavy element abundance. Below a certain threshold metallicity there would be insufficient building materials to form a terrestrial planet. Other literature sometime assume this threshold to be at $Z \geqslant 0.1Z_{\odot}$ (e.g. L01; P08), where stars would most likely struggle to build any planets. Hasegawa & Pudritz (2014) estimate the minimum metallicity for low-mass planets (as they define as $M_p \leqslant 30M_{\oplus}$) to form is [Fe/H] $\simeq -1.8$, although arguing that this number probably only serves as an upper limit to the minimum metallicity.

5.1.2 Semi-analytic Models

When we calculate the metallicity distributions from the semi-analytic models we divide the raw metallicity data from the models into bins with steps of Δ[Fe/H] $= 0.1$ dex. This choice of bin size is a bit of an exaggeration of the metallicity resolution from the Galacticus model, for which we have bins of twice that size. If we assume that our estimated metallicity distribution was wrong by a factor of ± 0.1 dex, our final results stay the same within a margin of two decimals. This is because most of the predicted mass formed by our estimates would still be confined to the metallicity range where the planet occurrence recipe predicts plentiful amount of terrestrial planets. The difference becomes greater if we limit the calculations to FGK-stars only however. This effect is most likely because of the enhanced sensitivity in the planet occurrence recipe for those type of stars (see e.g. Figure 3.8).

From the comparison of our two semi-analytic models and the literature in Sections 3.2.2 & 3.2.3, we note that the star formation rate of the Galacticus model is inconsistent with that of the best-fit function from the literature (Madau & Dickinson 2014) and the Durham model, albeit still within observational errors. The evolution of heavy elements in the Universe is also very different between the models. One might argue that due to the huge discrepancy between the two models, it is very improbable that they both reproduce the actual star formation history and chemical evolution of the Universe at the same time. We show that these two different models, one with quite similar star formation history as the literature and one with noticeably different, yield dissimilar results for both the number of terrestrial planets as well as the typical age. The star formation history from the literature and the Durham model predict the number of terrestrial planets in the observable Universe to be of order $\log_{10}(N_p) \sim 20.82 - 20.92$, with an average age of $\bar{t}_{\rm age} = 7.97 \pm 0.23$ Gyr. With the star formation history predicted by the Galacticus model however, the terrestrial planet population is $\sim 0.3 - 0.4$ dex higher and roughly one Gyr older.

The mass resolution of the Galacticus made it possible to include galaxies of lower mass ($\leqslant 10^7 M_\odot$) into our calculations. Due to the limitations of the simulation, the low-mass galaxies may not be very well resolved themselves and not act as ideal representatives of the galaxy population (A. Benson 2015, private communication). As it turns out, those galaxies are often extremely metal-deficient and thus unable to host terrestrial planets (see e.g. Figure 3.16). This is not very surprising as many low-mass galaxies become quenched in star formation quite early and do not produce many new stars that may enrich the coming generations with metals (Weisz et al. 2015). Regardless, the inclusion of low-mass galaxies is negligible compared to the amount of stars and terrestrial planets estimated from the high-mass galaxies.

An interesting result from our calculations is that if we compare the cosmic star formation rate with the planet formation rate, we get a slight delay in planet formation. This effect is also discussed by L01 and suggested to be because of the time needed for a sufficient growth of heavy elements to be able to produce planets. We estimate the offset in formation rates for our models to be $\sim 340 - 520$ Myrs. This delay in planet formation compared to star formation is lower than the $\sim 1.5 \pm 0.3$ Gyr L01 estimates. Our models predict terrestrial planets to be able to form very early on in the history of the Universe due to the anticipated development of heavy elements at a young cosmic age.

We illustrate this effect in Figure 5.1 where we plot the star formation rate, depicted by dashed lines, for both our semi-analytic models, the literature value from Equation 3.3 and L01. In the same plots we include the planet formation rates, shown as solid lines, which is the number of terrestrial planets formed per year per comoving Mpc^3. We also include a zoomed in version of all the star and planet formation rates together in the same plot where we scale the formation rates to the total amount of planets and stellar mass formed, seen in Figure 5.2. Same as in Figure 5.1, the dashed lines depicts the star formation rate and the solid lines the terrestrial planet formation rate (PFR).

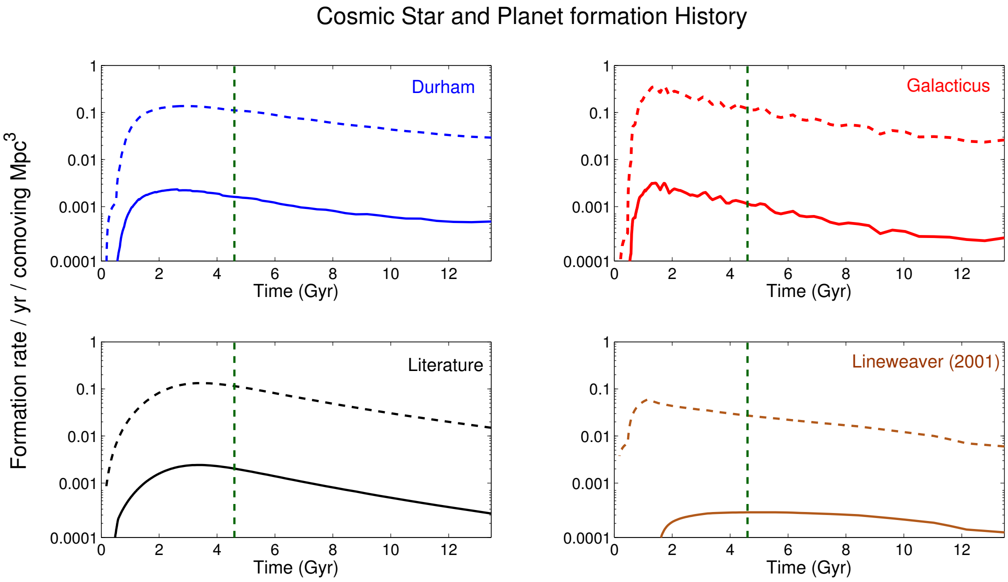

Figure 5.1: Cosmic formation rate for both stars (dashed) and terrestrial planets (solid) as function of time. The dark green dashed line indicate the time when the Sun formed. The blue and red lines show the formation rate calculated from the Durham and Galacticus semi-analytic models respectively. The black lines show the literature star formation rate from Equation 3.3 derived by Madau & Dickinson (2014) and the planet formation rate, which we estimate from the metallicity evolution described by Equation 3.4 from Kewley & Kobulnicky (2007). The brown lines show the formation rate we obtain if we apply the metallicity distribution and star formation rate that Lineweaver (2001) used. Note the earlier start for the star formation rates (dashed lines) in all of the plots compared to the planet formation rate. This effect is due to the need for a build up of heavier elements to make planets. The delay is less apparent for the Galacticus model where the chemical evolution is much higher at earlier times.

5.1.3 Stellar Characteristics

In our calculations we only consider stars on the main sequence to harbour terrestrial planets. We set our mass range of FGKM-stars to $M = 0.08 - 1.2M_{\odot}$, which is to try and be consistent with the earlier work of L01, albeit with the inclusion of low-mass M-dwarfs. We also argue for this spectral type range as the more extensive exoplanet

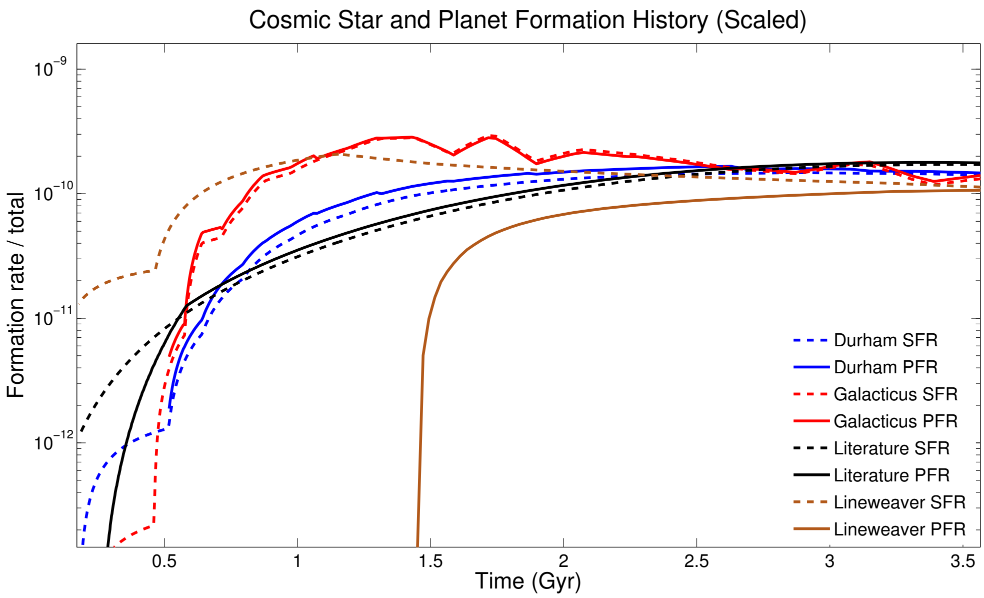

Figure 5.2: Cosmic formation history for both stars (dashed) and terrestrial planets (solid). Same as in Figure 5.1 but scaled to show the fraction of formation rate of the total amount of stellar mass and terrestrial planets formed. Note the offset for planet formation rate predicted by Lineweaver (2001) compared to the star formation rate, seen here by the brown lines. The build-up time for heavier elements required to produce terrestrial planets is $\sim 340 - 520$ Myr for our models. As the metallicity for the literature is calculated here with Equation 3.4, the onset for terrestrial planets begin ≈ 90 Myr after the first stars formed. With the planet occurrence recipe of Lineweaver (2001) where the minimum metallicity threshold is at [Fe/H]≈ -1, the delay for the literature metallicity to initiate terrestrial planet formation is increased to ≈ 630 Myrs.

missions survey these type of stars (e.g. *Kepler*, HARPS, CPS). Planets orbiting more evolved giant and subgiant stars have been observed however (e.g. Johnson et al. 2010, 2011; Veras et al. 2015). Theories also suggest that white dwarfs may be able to host planets without the need for capturing free floating planets (e.g. Veras et al. 2013). Observations of white dwarfs have indicated that the occurrence rate of planets orbiting white dwarfs is probably lower than that of main sequence Sun-like stars (Fulton et al. 2014). In our calculations we assumed all planets to be lost once the star moved on from the main sequence. As most of the planets in our estimates are harboured by very low-mass and long-lived M-dwarfs, the removal of planets orbiting FGK-stars no longer on the main sequence becomes insignificant.

Whether planets can form and survive in all environments in the Universe is unclear. Globular clusters were once thought most likely unable to host planets (Gonzalez et al. 2001), but later observations have detected several giant planets orbiting stars in globular clusters (e.g. Quinn et al. 2012). Simulations have also indicated that hot Jupiters could form quite easily in globular clusters (Shara et al. 2014). If scattering events due to gravitational interactions with nearby stellar companions are common in globular clusters, they may not be very hospitable to low-mass terrestrial planets. It has also been argued that elliptical galaxies may very well support accommodation of terrestrial planets in the habitable zone (Suthar & McKay 2012). We attempted to investigate if there was any difference between disk- or spheroid-dominated galaxies to harbour terrestrial planets (e.g Figure 3.16 and 3.20). For the Galacticus model we defined galaxies that were more massive in their disk part to be considered as disk-dominated and vice versa for spheroid-dominated. For the Durham model this was defined by the scale lengths instead, which is a less reliable approach due to scale lengths being dependent of how angular momentum is treated by the model. The results showed that most metal deficient and therefore planet-barren galaxies were low-mass disk-dominated galaxies whilst the most massive galaxies where spheroid-dominated and rich in metals. These results may be ameliorated by examining our method on individual galaxies with enhanced resolution.

In Section 3.1 we discuss the relation between stellar metallicity, mass and planet occurrence. Good measurements of the metallicity of stars can sometimes be difficult to obtain, especially for low-mass stars such as M-dwarfs (e.g. Casagrande et al. 2008). Other typical characteristics of stars may be better suited for determining the occurrence rates of planets, e.g. effective temperature (Howard et al. 2012).

5.1.4 Caveats

One of our major assumptions in this work is that giant planets on short orbits destroy low-mass planets during the migration phase of the giant planet. We assumed that low-mass planets were completely destroyed, not just ejected from the system and lost. Scattering events between planet-planet interactions are a plausible explanation to companions being ejected from a system and becoming free-floating planets that interact with neighbouring stars (Wang et al. 2015b). It has been suggested by e.g. Veras & Raymond (2012) that planet-planet scattering cannot alone explain the population of these *rogue* planets and give some other examples of how they might appear, e.g. forming via disk instabilities or representing the low-mass tail of the stellar initial mass function. We did not account for any possibility of rogue planets becoming entangled with stellar systems in our calculations.

The assumption that hot Jupiters are seldom accompanied by other planets only holds for other low-mass planets on short orbits. Surveys by Ngo et al. (2015); Wright et al.

(2009) present detections of giant planet companions to hot Jupiter hosts on very wide orbits, $\geqslant 50$ AU. These giant planets are not included into the planet occurrence recipe presented here as the power law adopted only observed giant planets on short orbits, $\leqslant 2.5$ AU. However, our assumption that all giant planets on orbits shorter than 2.5 AU removes all terrestrial planets is not iron-clad either. A few examples of multiplanetary systems with terrestrial planets orbiting on the inside of a giant planet companion have been detected (e.g. Gliese 676 system, Anglada-Escudé & Tuomi 2012). Simulations by e.g. Mandell et al. (2007) show that super-Earths might be able to form in the planetary disk after a hot Jupiter has swept by, although only in the habitable zone if no giant planet is present within $\leqslant 2.5$ AU. Therefore, our assumption that all giant planets destroy any prevalence of terrestrial planets may seem a bit strict. We probed the effect of having no giant planets to our calculations and gave the results in Table 4.2. We noted that due to the overall high probability for M-dwarf stars to form terrestrial planets as well as their shear number, the consequence of having no giant planets was not all too substantial. The effect was much stronger for FGK-stars where $\sim 20\%$ of the potential terrestrial planets were destroyed, also reducing the typical age by ~ 200 Myr.

There is also a question regarding "Good Jupiters". Planetary migration is not fully understood and indeed, we are in the presence of a Jupiter-sized planet that may have undergone a migration phase in the early solar system (see e.g. Agnor & Lin 2012). Yet, it stopped at a location where it is beneficial to our planet rather than destroying it. Evidently, not all giant planets undergo a voracious migration phase.

Another important issue to keep in mind is our scaling of the probability to form terrestrial planets orbiting M-dwarfs. As seen in Figure 3.8 and displayed by the dashed black line, the underlying probability (most noticeable at the lower metallicity end where giant planet formation is suppressed) to form terrestrial planets is scaled to the fit the occurrence rate of terrestrial planets orbiting M-dwarfs of $\lesssim 1$ from the solid line, describing the probability for Sun-like stars to form terrestrial planets of $\lesssim 0.4$. As this is done by simply rescaling and increasing the probability from the original probability to form terrestrials we used for Sun-like stars, we infer that the probability to form terrestrial planets is higher for low-mass stars with the same metallicity as their more massive counterparts. Since metallicity of a star is described by a fraction of its total mass, a low-mass star with the same [Fe/H] fraction as a high-mass star would actually have less total metal content. Our assumption here is that a low-mass M-dwarf would, even at the same metallicity, have an increased probability to form a terrestrial planet than a more massive star would. The question however, lies in whether the protoplanetary disk of a star with enough metals to form a number of planets will form several, smaller terrestrial planets or few, larger giant planets.

5.2 Summary

By combining results from interdisciplinary fields of astronomy such as exoplanet observations, planet formation theory, galaxy formation simulations and cosmology, we obtain means to estimate the number of terrestrial planets in the observable Universe. We summarise the results from our findings as following:

- By comparing the semi-analytic models with literature values we note that better constraints for simulations of galaxy formation on cosmic scales are essential for this purpose. The number of stars in the observable Universe and thus also the number of terrestrial planets can be modified by as much as a full order of magnitude depending on the star formation assumed. We find that the number of stars in observable Universe, $N_{*} \sim 9.57^{+2.63}_{-1.98} \times 10^{20}$ is somewhat lower than cruder estimates found on the web.
- Through our calculations we estimate the number of terrestrial planets in the observable Universe to be of the order of $\log_{10}(N_p) \geqslant 20.820^{+0.468}_{-0.001}$, with a typical age of $\bar{t}_{\rm age} \approx 7.94^{+1.13}_{-0.20}$ Gyr. We estimate the typical terrestrial planet to be older than that predicted of Earth-like planets by L01 by ≈ 1.5 Gyr and ≈ 3.3 Gyr older than the Earth. We estimate the number of terrestrial planets in the habitable zone ($\log_{10}(N_\eta) \geqslant 20.509^{+0.464}_{-0.003}$, with $\bar{t}_{\rm age} \approx 7.98^{+1.09}_{-0.23}$ Gyr) to be on the same order of magnitude as earlier estimates by Wesson (1990).
- By including low-mass stars as planet hosts we greatly increase the number of planets in the observable Universe. Our results imply a robust measurement for the number of terrestrial planets which does not vary much for different cosmic metallicity evolutions, nor when applying stricter constraints for the probability of stars to harbour them. Our results also suggest that Sun-like stars are more sensitive to variations in heavy element abundance in terms of being able to host terrestrial planets compared to low-mass stars. Furthermore, we obtain that the number of terrestrial planets destroyed by the presence of migrating giant planets is of the order of $\log_{10}(N_{\rm lost}) \approx 19.0$. We expect more stars to form giant planets that migrate than stars with inadequate materials to form terrestrial planets.
- Our results indicate that the observable Universe has been habitable for a very long time and that we expect terrestrial planets to abide in distant as well as

nearby galaxies. We also expect the more massive galaxies to harbour more and older planets per stellar mass than less massive galaxies.

- Our method is easily applied to single targeted galaxies (e.g. the Large Magellanic Cloud, see Section 4.3), provided sufficient data is available. Our models can also produce estimated values of the number of planets for Milky Way massive galaxies. Although, we argue for models of individual galaxy formation simulations to be able to make better assessments for this.
- Spheroid-dominated galaxies are presumed more likely to harbour terrestrial planets compared to disk-dominated galaxies according to our semi-analytic models.
- Including estimates of the number of planets in the observational regime, where we have confirmed detections of terrestrial planets, reveal that our planet occurrence recipe predicts ≈ 2.5 times more terrestrial planets than what is observed today.

The results we obtain can be used as a landmark for other similar studies using the same methodology. Our work also give semi-analytic models a new area to work with, as the results are very dependent on the performance of the simulations. A good representative model of the Milky Way would be very interesting to probe with our planet occurrence recipe, as the results could be beneficial for future exoplanet surveys in estimating which areas are most probable to harbour terrestrial sized planets.

5.2.1 Future Prospects

We believe all of our occurrence rate estimates to improve with the aid of current and future space missions, e.g. the K2 mission (Howell et al. 2014), the TESS mission (Ricker et al. 2014) and the PLATO mission (Rauer et al. 2014). Expanded searches for exoplanets targeting stars of a broader variety will help refining the current interpretation of potential terrestrial planet hosts. Observations of protoplanetary disks at different stages may provide better constraints to planet formation theories for host stars of varying mass and metallicity. We also expect additional developments in galaxy formation and high-redshift observations will aid in placing further constraints on the star formation history and chemical evolution of the Universe, thus also benefiting our estimates.

This research has made use of the Exoplanet Orbit Database and the Exoplanet Data Explorer at exoplanets.org.

Bibliography

Agnor, C. B. & Lin, D. N. C. 2012, ApJ, 745, 143

Angerhausen, D., Sapers, H., Simoncini, E., et al. 2014, in IAU Symposium, Vol. 293, IAU Symposium, ed. N. Haghighipour, 192–196

Anglada-Escudé, G. & Tuomi, M. 2012, A & A, 548, A58

Armitage, P. J. 2003, ApJL, 582, L47

Armitage, P. J. 2007, ArXiv Astrophysics e-prints

Armitage, P. J. & Rice, W. K. M. 2005, ArXiv Astrophysics e-prints

Badescu, V. 2011, Icarus, 216, 485

Barger, A. J., Cowie, L. L., & Richards, E. A. 2000, AJ, 119, 2092

Batalha, N. M. 2014, Proceedings of the National Academy of Science, 111, 12647

Batygin, K. & Laughlin, G. 2015, Proceedings of the National Academy of Science, 112, 4214

Baugh, C. M. 2006, Reports on Progress in Physics, 69, 3101

Benítez-Llambay, P., Masset, F., Koenigsberger, G., & Szulágyi, J. 2015, Nature, 520, 63

Benson, A. 2011, Galacticus: A Semi-Analytic Model of Galaxy Formation, Astrophysics Source Code Library

Boley, A. C. 2009, ApJL, 695, L53

Bonfils, X., Delfosse, X., Udry, S., et al. 2013, A & A, 549, A109

Borucki, W. J., Koch, D. G., Basri, G., et al. 2011, ApJ, 736, 19

Boss, A. P. 1997, Science, 276, 1836

Boss, A. P. 2010, in IAU Symposium, Vol. 265, IAU Symposium, ed. K. Cunha, M. Spite, & B. Barbuy, 391–398

Bouwens, R. J., Illingworth, G. D., Oesch, P. A., et al. 2012a, ApJ, 754, 83

Bouwens, R. J., Illingworth, G. D., Oesch, P. A., et al. 2012b, ApJL, 752, L5

Boylan-Kolchin, M., Springel, V., White, S. D. M., Jenkins, A., & Lemson, G. 2009, MNRAS, 398, 1150

Bressan, A., Marigo, P., Girardi, L., et al. 2012, MNRAS, 427, 127

Bromley, B. C. & Kenyon, S. J. 2015, ArXiv e-prints

Buchhave, L. A., Bizzarro, M., Latham, D. W., et al. 2014, Nature, 509, 593

Buchhave, L. A., Latham, D. W., Johansen, A., et al. 2012, Nature, 486, 375

Butler, R. P., Vogt, S. S., Marcy, G. W., et al. 2000, ApJ, 545, 504

Campante, T. L., Barclay, T., Swift, J. J., et al. 2015, ApJ, 799, 170

Casagrande, L., Flynn, C., & Bessell, M. 2008, MNRAS, 389, 585

Cassan, A., Kubas, D., Beaulieu, J.-P., et al. 2012, Nature, 481, 167

Chabrier, G. 2003, Publications of the ASP, 115, 763

Chatterjee, S., Ford, E. B., Matsumura, S., & Rasio, F. A. 2008, ApJ, 686, 580

Clanton, C. & Gaudi, B. S. 2014, ApJ, 791, 91

Cochran, W. D., Endl, M., Wittenmyer, R. A., & Bean, J. L. 2007, ApJ, 665, 1407

Cockell, C. S. 2014, International Journal of Astrobiology, 13, 158

Cole, S., Lacey, C. G., Baugh, C. M., & Frenk, C. S. 2000, MNRAS, 319, 168

Cossou, C., Raymond, S. N., Hersant, F., & Pierens, A. 2014, A & A, 569, A56

Cucciati, O., Tresse, L., Ilbert, O., et al. 2012, AaP, 539, A31

D'Angelo, G., Durisen, R. H., & Lissauer, J. J. 2010, Giant Planet Formation, ed. S. Seager, 319–346

Dawson, R. I. & Murray-Clay, R. A. 2013, ApJL, 767, L24

Dominik, M. 2012, Acta Astronautica, 78, 99

Doyle, L. R., Carter, J. A., Fabrycky, D. C., et al. 2011, Science, 333, 1602

Dressing, C. D. & Charbonneau, D. 2013, ApJ, 767, 95

Dressing, C. D. & Charbonneau, D. 2015, ArXiv e-prints

Farr, W. M., Mandel, I., Aldridge, C., & Stroud, K. 2014, ArXiv e-prints

Fischer, D. A. & Valenti, J. 2005, ApJ, 622, 1102

Ford, E. B. 2014, Proceedings of the National Academy of Science, 111, 12616

Fressin, F., Torres, G., Charbonneau, D., et al. 2013, ApJ, 766, 81

Fulton, B. J., Tonry, J. L., Flewelling, H., et al. 2014, ApJ, 796, 114

Gaidos, E. & Mann, A. W. 2014, ApJ, 791, 54

Gallazzi, A., Brinchmann, J., Charlot, S., & White, S. D. M. 2008, MNRAS, 383, 1439

Gaudi, B. S., Albrow, M. D., An, J., et al. 2002, ApJ, 566, 463

Giavalisco, M., Dickinson, M., Ferguson, H. C., et al. 2004, ApjL, 600, L103

Gilliland, R. L., Brown, T. M., Guhathakurta, P., et al. 2000, ApJL, 545, L47

Goldblatt, C. 2015, ArXiv e-prints

Gonzalez, G. 2000, in Astronomical Society of the Pacific Conference Series, Vol. 219, Disks, Planetesimals, and Planets, ed. G. Garzón, C. Eiroa, D. de Winter, & T. J. Mahoney, 523

Gonzalez, G. 2005, Origins of Life and Evolution of the Biosphere, 35, 555

Gonzalez, G. 2014, ArXiv e-prints

Gonzalez, G., Brownlee, D., & Ward, P. 2001, Icarus, 152, 185

Gummersbach, C. A., Kaufer, A., Schaefer, D. R., Szeifert, T., & Wolf, B. 1998, A & A, 338, 881

Guo, J., Zhang, F., Chen, X., & Han, Z. 2009, Astrophysics and Space Science, 323, 367

Guo, J., Zhang, F., & Han, Z. 2010, Astrophysics and Space Science, 327, 233

Han, E., Wang, S. X., Wright, J. T., et al. 2014, Publications of the ASP, 126, 827

Hasegawa, Y. & Pudritz, R. E. 2014, ApJ, 794, 25

Heller, R., Williams, D., Kipping, D., et al. 2014, Astrobiology, 14, 798

Helly, J. C., Cole, S., Frenk, C. S., et al. 2003, MNRAS, 338, 913

Henriques, B. M. B., Thomas, P. A., Oliver, S., & Roseboom, I. 2009, MNRAS, 396, 535

Hinkel, N. R. & Kane, S. R. 2013, ApJ, 774, 27

Hopkins, A. M. 2004, ApJ, 615, 209

Hopkins, A. M. & Beacom, J. F. 2006, ApJ, 651, 142

Howard, A. W., Marcy, G. W., Bryson, S. T., et al. 2012, ApJs, 201, 15

Howell, S. B., Sobeck, C., Haas, M., et al. 2014, PASP, 126, 398

Ida, S. & Lin, D. N. C. 2004, ApJ, 616, 567

Jetzer, P. 2008, in Manchester Microlensing Conference, 43

Johnson, J. A., Aller, K. M., Howard, A. W., & Crepp, J. R. 2010, Publications of the ASP, 122, 905

Johnson, J. A., Clanton, C., Howard, A. W., et al. 2011, ApJs, 197, 26

Joshi, M. M., Haberle, R. M., & Reynolds, R. T. 1997, Icarus, 129, 450

Kasting, J. F., Whitmire, D. P., & Reynolds, R. T. 1993, Icarus, 101, 108

Kewley, L. & Kobulnicky, H. A. 2007, The Metallicity History of Disk Galaxies, ed. R. S. DE JONG, 435

Kewley, L. J. & Ellison, S. L. 2008, ApJ, 681, 1183

Kim, S., Staveley-Smith, L., & Dopita, M. A. 1998, in Magellanic Clouds and Other Dwarf Galaxies, ed. T. Richtler & J. M. Braun, 169–172

Kley, W. & Nelson, R. P. 2012, Annual Review of Astron and Astrophys, 50, 211

Kopparapu, R. K. 2013, ApJL, 767, L8

Kopparapu, R. K., Ramirez, R., Kasting, J. F., et al. 2013, ApJ, 765, 131

Kroupa, P. 2001, MNRAS, 322, 231

Kroupa, P. 2002, Science, 295, 82

Lanzetta, K. M., Yahata, N., Pascarelle, S., Chen, H.-W., & Fernández-Soto, A. 2002, ApJ, 570, 492

Latham, D. W., Rowe, J. F., Quinn, S. N., et al. 2011, ApJL, 732, L24

Licquia, T. & Newman, J. 2013, in American Astronomical Society Meeting Abstracts, Vol. 221, American Astronomical Society Meeting Abstracts #221, 254.11

Lin, D. N. C., Bodenheimer, P., & Richardson, D. C. 1996, Nature, 380, 606

Lineweaver, C. H. 2001, Icarus, 151, 307

Lineweaver, C. H., Fenner, Y., & Gibson, B. K. 2004, Science, 303, 59

Lissauer, J. J., Dawson, R. I., & Tremaine, S. 2014, Nature, 513, 336

Lovis, C. & Fischer, D. 2010, Radial Velocity Techniques for Exoplanets, ed. S. Seager, 27–53

Luger, R. & Barnes, R. 2015, Astrobiology, 15, 119

Madau, P. & Dickinson, M. 2014, Annual Review of Astron and Astrophys, 52, 415

Mandell, A. M., Raymond, S. N., & Sigurdsson, S. 2007, ApJ, 660, 823

Mann, A. W., Gaidos, E., & Ansdell, M. 2013, ApJ, 779, 188

Marcy, G. W. & Butler, R. P. 2000, Publications of the ASP, 112, 137

Marcy, G. W., Isaacson, H., Howard, A. W., et al. 2014, ApJs, 210, 20

Mayor, M. & Queloz, D. 1995, Nature, 378, 355

McMillan, P. J. 2011, MNRAS, 414, 2446

Montet, B. T., Crepp, J. R., Johnson, J. A., Howard, A. W., & Marcy, G. W. 2014, ApJ, 781, 28

Mulders, G. D., Pascucci, I., & Apai, D. 2015, ApJ, 798, 112

Mullally, F., Coughlin, J. L., Thompson, S. E., et al. 2015, ApJs, 217, 31

Murray, N., Paskowitz, M., & Holman, M. 2002, ApJ, 565, 608

Mustill, A. J., Davies, M. B., & Johansen, A. 2015, ArXiv e-prints

Nagamine, K., Fukugita, M., Cen, R., & Ostriker, J. P. 2001, ApJ, 558, 497

Neves, V., Bonfils, X., Santos, N. C., et al. 2013, A & A, 551, A36

Ngo, H., Knutson, H. A., Hinkley, S., et al. 2015, ApJ, 800, 138

Noack, L., Godolt, M., von Paris, P., et al. 2014, Planet. Space Sci., 98, 14

Petigura, E. A., Howard, A. W., & Marcy, G. W. 2013, Proceedings of the National Academy of Science, 110, 19273

Petrovich, C. 2015, ApJ, 799, 27

Piatti, A. E. & Geisler, D. 2013, AJ, 145, 17

Prantzos, N. 2008, Space Sci Rev, 135, 313

Quinn, S. N., White, R. J., Latham, D. W., et al. 2012, ApJL, 756, L33

Quintana, E. V., Barclay, T., Raymond, S. N., et al. 2014, Science, 344, 277

Rauer, H., Catala, C., Aerts, C., et al. 2014, Experimental Astronomy, 38, 249

Ricker, G. R., Winn, J. N., Vanderspek, R., et al. 2014, in Society of Photo-Optical Instrumentation Engineers (SPIE) Conference Series, Vol. 9143, Society of Photo-Optical Instrumentation Engineers (SPIE) Conference Series, 20

Rocha-Pinto, H. J. & Maciel, W. J. 1996, MNRAS, 279, 447

Rocha-Pinto, H. J., Scalo, J., Maciel, W. J., & Flynn, C. 2000, AaP, 358, 869

Rolleston, W. R. J., Smartt, S. J., Dufton, P. L., & Ryans, R. S. I. 2000, A & A, 363, 537

Rushby, A. J., Claire, M. W., Osborn, H., & Watson, A. J. 2013, Astrobiology, 13, 833

Scalo, J., Kaltenegger, L., Segura, A. G., et al. 2007, Astrobiology, 7, 85

Segura, A., Kasting, J. F., Meadows, V., et al. 2005, Astrobiology, 5, 706

Selsis, F., Kasting, J. F., Levrard, B., et al. 2007, A & A, 476, 1373

Sengupta, S. 2015, ArXiv e-prints

Shara, M. M., Hurley, J. R., & Mardling, R. A. 2014, ArXiv e-prints

Sleep, N. H. 2005, Annual Review of Earth and Planetary Sciences, 33, 369

Sommer-Larsen, J. 1991, MNRAS, 249, 368

Soubiran, C., Bienaymé, O., Mishenina, T. V., & Kovtyukh, V. V. 2008, A & A, 480, 91

Sparke, L. & Gallagher, J. 2007, Galaxies in the Universe: An Introduction (Cambridge University Press)

Springel, V., White, S. D. M., Jenkins, A., et al. 2005, Nature, 435, 629

Steffen, J. H., Ragozzine, D., Fabrycky, D. C., et al. 2012, Proceedings of the National Academy of Science, 109, 7982

Stringer, M. J., Brooks, A. M., Benson, A. J., & Governato, F. 2010, MNRAS, 407, 632

Suthar, F. & McKay, C. P. 2012, International Journal of Astrobiology, 11, 157

Swift, J. J., Johnson, J. A., Morton, T. D., et al. 2013, ApJ, 764, 105

Tackley, P. J., Ammann, M. M., Brodholt, J. P., Dobson, D. P., & Valencia, D. 2014, in IAU Symposium, Vol. 293, IAU Symposium, ed. N. Haghighipour, 339–349

Tuomi, M., Jones, H. R. A., Barnes, J. R., Anglada-Escudé, G., & Jenkins, J. S. 2014, MNRAS, 441, 1545

Veras, D., Eggl, S., & Gaensicke, B. T. 2015, ArXiv e-prints

Veras, D., Mustill, A. J., Bonsor, A., & Wyatt, M. C. 2013, MNRAS, 431, 1686

Veras, D. & Raymond, S. N. 2012, MNRAS, 421, L117

Visbal, E., Barkana, R., Fialkov, A., Tseliakhovich, D., & Hirata, C. M. 2012, Nature, 487, 70

Wang, J., Fischer, D. A., Horch, E. P., & Huang, X. 2015a, ApJ, 799, 229

Wang, L., Kouwenhoven, M. B. N., Zheng, X., Church, R. P., & Davies, M. B. 2015b, MNRAS, 449, 3543

Ward, W. R. 1997, Icarus, 126, 261

Weisz, D. R., Dolphin, A. E., Skillman, E. D., et al. 2015, ArXiv e-prints

Wesson, P. S. 1990, QJRAS, 31, 161

Wolf, A. S., Laughlin, G., Henry, G. W., et al. 2007, ApJ, 667, 549

Wolszczan, A. & Frail, D. A. 1992, Nature, 355, 145

Wright, E. L. 2006, Publications of the ASP, 118, 1711

Wright, J. T., Fischer, D. A., Ford, E. B., et al. 2009, ApJL, 699, L97

Yang, J., Boué, G., Fabrycky, D. C., & Abbot, D. S. 2014a, ApJL, 787, L2

Yang, J., Cowan, N. B., & Abbot, D. S. 2013, ApJL, 771, L45

Yang, J., Liu, Y., Hu, Y., & Abbot, D. S. 2014b, ApJL, 796, L22